Arabian Journal of Geosciences (2022) 15: 812
https://doi.org/10.1007/s12517-022-09934-2

ORIGINAL PAPER

A new approach for physically based probabilistic seismic hazard analyses for Portugal

Enrico Zacchei[1,2] · **Reyolando Brasil**[3,4]

Received: 19 August 2021 / Accepted: 15 March 2022 / Published online: 19 April 2022

Abstract

Probabilistic seismic hazard analysis (PSHA) is nowadays the more complete analysis method to estimate the seismic input for structural analysis. However, it is strongly influenced by seismogenic parameters and attenuation equations. Here PSHA using empirical Green's functions (EGFs) with 2 + 2 variables is carried out, which, as proposed, are related to each other through the moment magnitude. This combination, already known as "physically based PSHA (pb-PSHA)," is an approach that should be disseminated since it could provide a good alternative in countries where the seismogenic zones and/or attenuation equations are not well established. The proposed model, using differential equations, is based on a linear fault, random/periodic/impulsive/linear source functions, and punctual hypocenter. Results are shown in terms of new seismic parameters, specific return periods, and ground accelerations. The studied country is Portugal since it appears to the authors that no study has been published about pb-PSHA for Portugal. In this sense, the model could be of importance for hazard analyses to incentivize more research on the earthquake source physics.

Keywords PSHA · EGF · Pb-PSHA for Portugal · Seismic analysis

Introduction

Background

The definition of correct seismic inputs has always been of interest for both geophysicists and engineers in different parts of the world, for instance, in Portugal (Carvalho 2007; Goff et al. 2014), Spain (Zacchei et al. 2017; Peláez et al. 2005), Italy (Faccioli and Paolucci 2005; Sabetta et al. 2005), Pakistan (Qadri and Malik 2021; Qadri et al. 2015a, 2017, 2015b), India (Putti and Satyam 2020), and Bangladesh (Ansary and Arefin 2020).

Responsible editor: Longjun Dong.

✉ Enrico Zacchei
enricozacchei@gmail.com

1 Itecons, Coimbra, Portugal

2 University of Coimbra, CERIS, Coimbra, Portugal

3 Polytechnic School of São Paulo, University of São Paulo (USP), 380 Prof. Luciano Gualberto, São Paulo, SP, Brazil

4 Center for Engineering, Modeling and Applied Social Sciences, Federal University of ABC (UFABC), 3 Rua Arcturus, São Bernardo do Campo, SP, Brazil

There are several procedures that provide seismic inputs for structure designing. These procedures can be deterministic by using elastic spectra from codes (Ministerio delle Infrastructure 2008; Committee and for Standardization (CEN), Design of structures for earthquake resistance, Part 1: General rules, seismic actions and rules for buildings, 2004;), synthetic spectra by attenuation equations (Carvalho 2007; Goff et al. 2014), seismic hazard analyses (Zacchei et al. 2017; Pailoplee et al. 2009), artificial accelerograms obtained from power spectrum density functions (Barone et al. 2015; Zacchei and Molina 2018), seismic coefficients by amplification of inertial forces (Ministério da Habilitação 1983), time-history analyses from database (Portuguese Institute of Sea and Atmosphere (IPMA) http://www.ipma.pt/pt/geofisica/sismicidade/; Luzi et al. 2016), and spectrum compatible analyses by scaling factor (Jayaram et al. 2011; Soysal et al. 2017; Valentini et al. 2019).

The probabilistic procedures can be the probabilistic seismic hazard analysis (PSHA) by Cornel model (Cornell 1968) and the physically based PSHA (pb-PSHA) (Mert et al. 2016; Hutching et al. 2017), which is treated in this paper. These probabilistic methods allow to define an estimation of the mean probability (over space and time) of the occurrence of a seismic event with a certain magnitude within a given time interval.

The pb-PSHA is mainly based on the PSHA, which is nowadays the more complete method to estimate the seismic input because it accounts for the seismotectonic and geological context and the probability of occurrence of earthquakes (Zacchei et al. 2017; Sabetta et al. 2005; Mulargia et al. 2017; Chan et al. 2013; Kutanis et al. 2018; Ahulu et al. 2018; Silacheva et al. 2018; Valentini et al. 2019).

Pb-PSHA follows the same procedures of standard PSHA with only one difference: attenuation equations are not used, and they are substituted by empirical Green's functions (EGFs) and computation of physically based seismograms and direct analysis accounting the hazard for structures (Fergany and Hutchings 2017).

EGFs allow to directly calculate the ground displacement at a site, defining wave paths from a certain seismic source to the ground. As mentioned in Lior and Ziv (2018) "resolving earthquake source parameters is key for addressing fundamental questions in earthquake science." However, it is very difficult to know the correct characteristic of the soil to quantify possible amplifications of the wave (Nacional and de Informação de Recursos Hidricos (SNIRH), database. 2020).

Also, it is difficult to predict the effects in function of the source-site distance. In fact, the earthquake-induced seismic hazard is uneven in spatial distribution; therefore, after an earthquake occurs, the degree of disaster may vary greatly at the same distance but in different directions as studied in Denolle et al. (2018); Ma et al. 2019b).

In (Lior and Ziv 2018) new interesting relations between the peak ground acceleration (PGA) and earthquake source parameters have been introduced showing an easy implementation also for low-seismicity regions. In (Ma et al. 2019a) it is mentioned that "ground motion prediction methodologies without any accounting for the source factors will simply be inadequate."

In the modern approach shown in Poljansek et al. (2017), it is put to attention the correct definition of seismic hazard, which with the vulnerability and exposure analyses, a global risk analysis is found as studied in Zacchei and Molina (2021). Also, the correct identification of the model and parameters to be used is an important aspect.

A possible issue is to choose a consistent model and parameters (random and epistemic) to be correctly used. "Random" uncertainties are related to the inherent randomness of the studied phenomena, whereas the "epistemic" uncertainties are related to the lack of knowledge of the models (Hariri-Ardebili and Saouma 2016; Zacchei and Molina 2020). Random and epistemic uncertainties are studied in stochastic analyses, which are used to solve problems that cannot be deterministically solved because models are not completely known, or data are not available (Zacchei and Molina 2021; Yan et al. 2016; Dong et al. 2017). However, when epistemic uncertainties are predominant with respect to random uncertainties, it is difficult to choose a unique model.

The studied area in this paper is Portugal where seismic activity is high as shown in Fig. 1. The total average annual loss in Portugal, which "represents the long-term mean loss value per year due to direct damage caused by earthquake ground shaking in the residential, commercial, and industrial building stock, considering structural and non-structural components and building contents" is 69.0×10^6 \$ (Global earthquake model (GEM), database, Accessed in 10, 2020. Available online: https://www.globalquakemodel.org/gem).

Since the 1755 Lisbon earthquake to the more recent great earthquake 1998 Azores-Faial (Global earthquake model (GEM), database, Accessed in 10, 2020. Available online: https://www.globalquakemodel.org/gem), several studies, including old ones (example from the Spanish coast 2001; Gràcia et al. 2003; Gutscher et al. 2006; Thiebot and Gutscher 2006) up to the most recent (Cunha et al. 2012; Matias et al. 2013; Woessner et al. 2015), have been developed. For Portugal, some papers have been published about PSHA (Carvalho 2007; Carvalho and Malfeito 2018; Carvalho et al. 2018; Sousa and Costa 2009) but it appears to the authors that no study has been published about pb-PSHA.

Motivation of this study

The motivations of this study are summarized in the following points.

1. Lack of a well-calibrated attenuation equation for Portugal. To the best of the authors' knowledge, there are four attenuation laws for Portugal of which three are expressed in terms of seismic intensity due to the scarcity of instrumental data (Jiménez and García-Fernández 1999; Goff et al. 2014; Sousa and Oliveira 1997) and one is expressed in terms of spectral accelerations (Carvalho 2007) (see Table 1). These equations are very different from each other although they should be used for the same country. In this sense they could not be fully reliable.

2. There are four valid models for Portugal that characterize the seismogenic zones (ZSs): Share, Ersta, EC8, and Zesis (IGME 2015; Carvalho and Malfeito 2018; Committee and for Standardization (CEN), Design of structures for earthquake resistance, Part 1: General rules, seismic actions and rules for buildings 2004;) (see

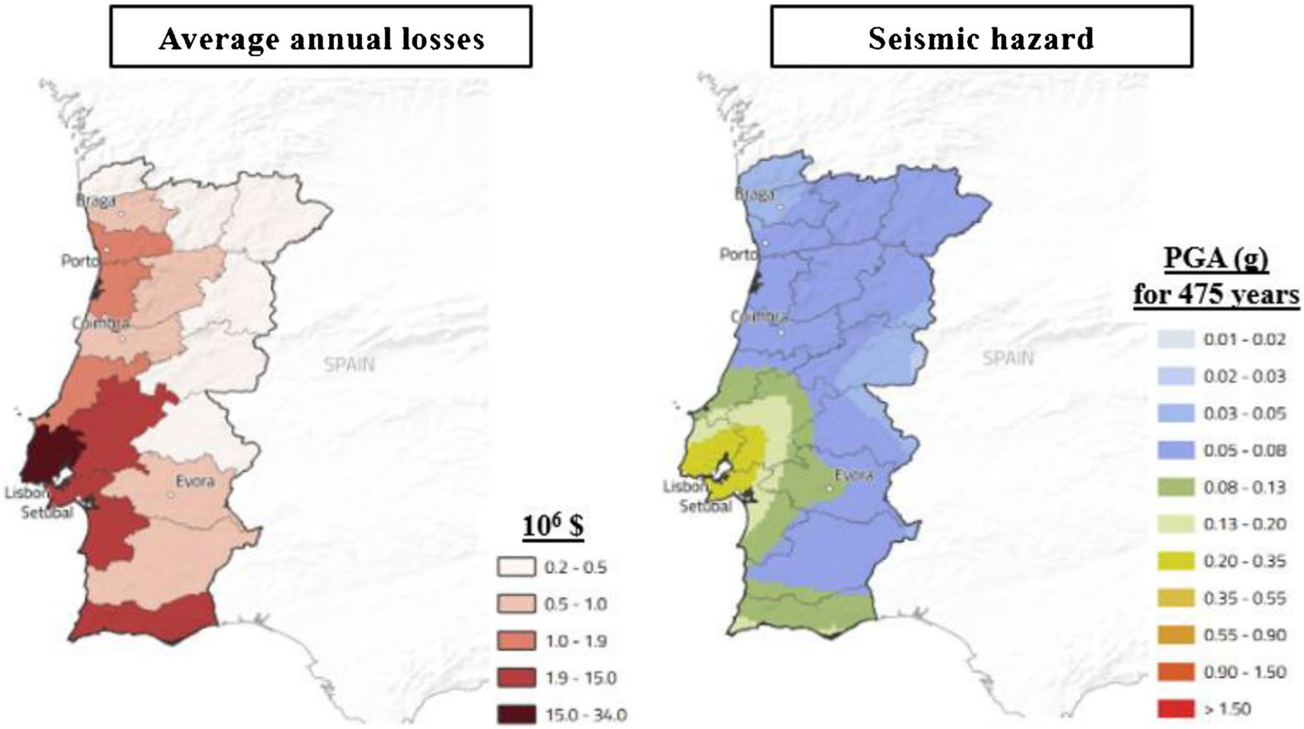

Fig. 1 Portugal maps: average annual losses and seismic hazard (modified from Global earthquake model (GEM), database, Accessed in 10, (2020). Available online: https://www.globalquakemodel.org/gem)

Table 1 Attenuation equations for Portugal[a]

Attenuation equation	Year
$I = 0.98 + 0.85\ \mathrm{M} - 0.23\ \mathrm{In}\ (R) - 0.006\ R^{b}$	1997 (Sousa and Oliveira 1997)
$I = 6.8 + 1.13\ \mathrm{M} - 1.68\ \mathrm{In}\ (R + 14)$	1999 (Jiménez and García-Fernández 1999)
$\log_{10}\mathrm{PGA} = -0.74 + 0.55\ \mathrm{M} - 0.002\ \log_{10} R - 0.61\ R + 0.25$	2007 (Carvalho 2007)
$I = -1.9438\ \mathrm{In}\ (R) + 4.1\ \mathrm{M} - 9.5763$	2014 (Goff et al. 2014)

I intensity, *M* considered magnitude, considered distance, *PGA* peak ground acceleration.

[a]In (Douglas 2019; Ambraseys et al. 2005), other attenuation equations calibrated by using Portugal data are presented; however, these are not strictly defined for this country.

[b]Values estimated for a specific zone: ZS5 for EC8 model (see Fig. 2).

Fig. 2). These models can provide different outputs as shown in literature (Carvalho and Malfeito 2018; Sousa and Costa 2009; Sousa and Oliveira 1997; Fonseca et al. 2011) whereby using the same ZSs for the EC8 model different values are obtained.

3. Inconsistency of the following relation: $\mathrm{PGA} = \gamma_I \times \mathrm{PGA}_R$, where γ_I is the importance factor and PGA_R is the reference PGA (Ministerio delle Infrastructure 2008; Committee and for Standardization (CEN), Design of structures for earthquake resistance, Part 1: General rules, seismic actions and rules for buildings 2004; Sousa et al. 2019). This relation correlates an acceleration (PGA) with the type of construction. As mentioned in Sousa et al. (2019); García-Pérez et al. 2005), γ_I is not related to the structure characteristics; therefore, this relation should be inconsistent. Thus, the logic to correlate the structure (object to be designed at surface) with a PGA (seismic input in deep) should be exceeded.

A more correct form to quantify the importance factor has been treated in literature where this factor is calibrated as a function of the vulnerability of the structures, external loadings (Kodur and Naser 2013), evaluation of benefit/costs for the service life (García-Pérez et al. 2005), losses due to damage and failure of the structure (Pozos-Estrada et al. 2016), and accounting hazard/vulnerability/exposure in a unique solution (Zacchei and Molina 2021).

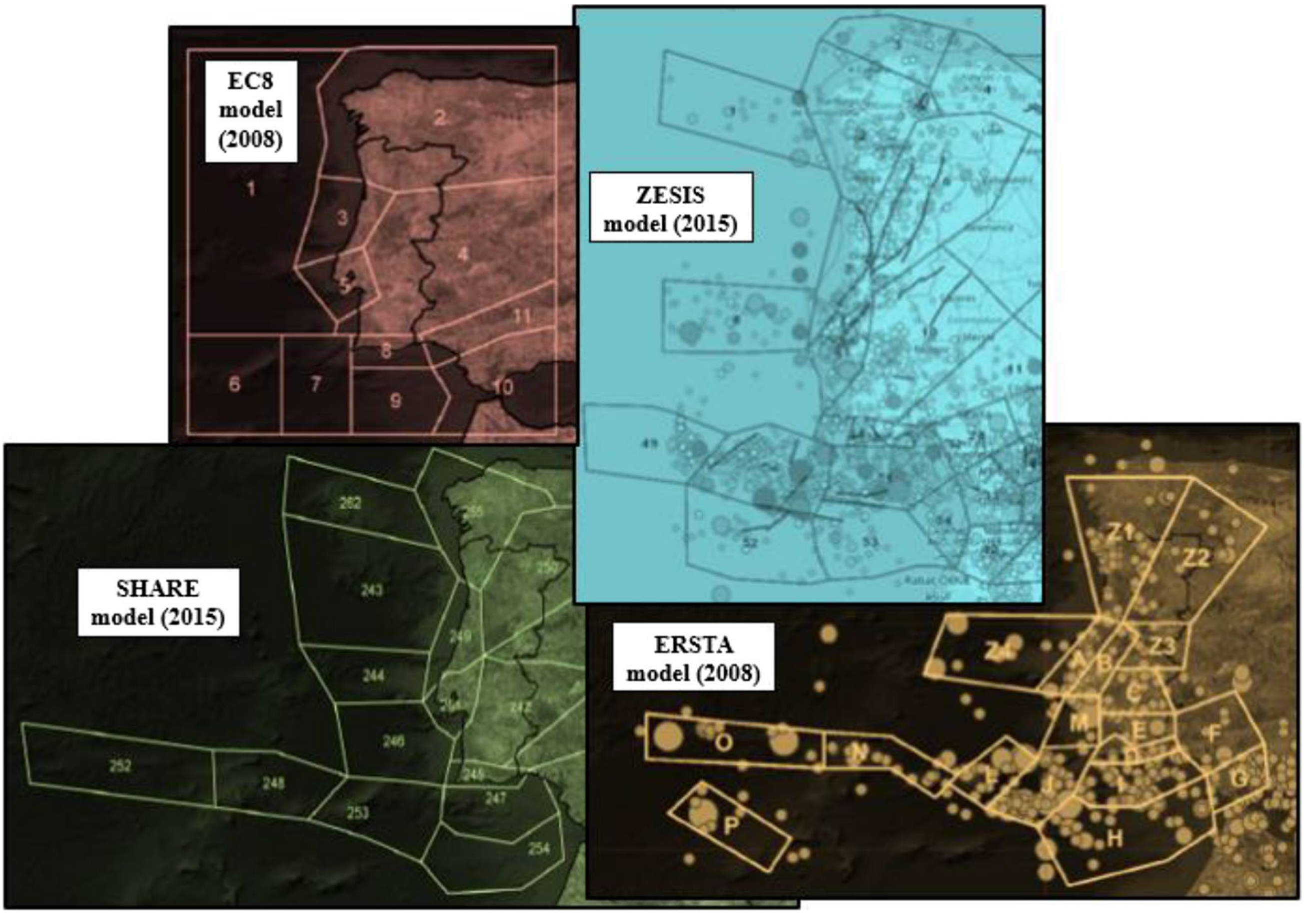

Fig. 2 Seismogenic zones for Portugal: Share, Ersta, EC8, and Zesis (modified from IGME (2015); Carvalho and Malfeito 2018; Committee and for Standardization (CEN), Design of structures for earthquake resistance, Part 1: General rules, seismic actions and rules for buildings 2004))

Therefore, in this paper a model for pb-PSHA using EGFs is proposed without using an attenuation equation. Both models are related to each other through the moment magnitude M_w. The seismic source is idealized by random, impulsive, periodic, and linear function to estimate the PGAs. Also, a comparison between ZS models has been carried out to identify the discrepancies and "ad hoc" return periods.

Materials

Materials for the seismic hazard

Four seismogenic zones (ZSs) have been selected of which two are typically used only for Portugal, i.e., the Share and Ersta (Carvalho and Malfeito 2018) zones. Other ones are the Eurocode EC8 (Carvalho and Malfeito 2018; Committee and for Standardization (CEN), Design of structures for earthquake resistance, Part 1: General rules, seismic actions and rules for buildings, 2004;) and the Iberian Peninsula Zesis (IGME 2015).

From these ZSs, some data have been collected and used to calibrate new values regarding 6 specific ZSs. This data analysis is based on associated events that characterize the seismicity of each seismogenic zone for Zesis. The group of events has been divided in sub-groups, ΔM_w, associated to a number of events with the same moment magnitude, M_w, completeness period, completeness interval, frequency of events of similar intensity, mean annual rate of exceedance, λ_c.

The events provided by Zesis have already been processed for homogenization, declustering, and completeness (Faccioli and Paolucci 2005; Zacchei et al. 2017). Therefore, these operations have not been repeated in this paper. Thus, all events have been taken as they are with the registered M_w and, for the completeness period, the oldest year has been considered.

The values of λ_c for events with magnitude M_w are correlated by the well-known Gutenberg-Richter (G&R) law (Zhan 2017; Wu et al. 2018), where the slope, *b*-value, describes the ratio between the number of small and large events, whereas the $\log_{10}(\lambda_c)$ intercept, *a*-value, measures the level of seismicity (or "productivity" as mentioned in Gulia and Wiemer (2019)).

Table 2 shows the selected ZSs regarding continental Portugal and the equivalence between them in terms of nomenclatures.

It is possible to see that the ZSs for EC8 include more than one of ZSs for other models, as for instance, the 4 and 2 zones. This is expected since the EC8 zones are very large as shown in Fig. 2.

Table 3 lists the parameters collected from literature and obtained in this analysis where it is possible to see that *b*-value ranges from 0.64 to 1.06. *b*-value is considered as the universality value, i.e., considering the reference value $b = 1.0$, when $b < 1.0$ the area is more dominated by large but infrequent events and the small earthquakes have a lower frequency compared to the strong earthquakes (Wu et al. 2018).

In Table 3, for EC8 model, two different values for each ZS are shown (Carvalho and Malfeito 2018; Sousa and Costa 2009; Sousa and Oliveira 1997; Fonseca et al. 2011), where the total mean difference is ~ 7%. This could confirm the difficulty in estimating a unique value, although the model and the correlated area are the same.

A difference between a mean of *b*-values calculated by Share, Zesis, Ersta, and EC8 models and the *b*-values calculated in this analysis is 0.033 (3.75% error) indicating a good agreement.

Figure 3 shows the G&R trend for each ZS for Zesis. The solid line is the R&G trend with $b = 1.0$ (Bentz et al. 2020). The horizontal difference between each point of the same ZS represents the pre-defined sub-groups ΔM_w (as shown in Fig. 3 for the ZS7 example). In fact, this difference maintains constant.

Table 4 shows *a*-values for all models. The range of *a*-value is 2.27–3.60. In fact, *a*-values are generally of the order of 3.0 as indicated in Eurocode (Committee and for Standardization (CEN), Design of structures for earthquake resistance, Part 1: General rules, seismic actions and rules for buildings, 2004). Obtaining a good agreement for *a*-values is more complicated since a small variation of *b*-values provides a large variation of *a*-values at $M_w = 0$. Here the estimated difference is 0.252 (9.09% error).

Finally, Table 5 shows λ_c values only for models with available data. This parameter, which ranges between 0.04 and 0.32, is strongly influenced by the number of events to be considered with the same M_w. Here a poor agreement is obtained, with a difference of 0.07 (47% error); however,

Table 2 Equivalences between the seismogenic zones (ZSs)

ZS for Share (Carvalho and Malfeito 2018)	ZS for Zesis (IGME 2015)	ZS for Ersta (Carvalho and Malfeito 2018)	ZS for EC8 (Carvalho and Malfeito 2018)
242 (Évora)[a]	10	C, E, and Z3	4
245 (Algarve)	13	D	8
249 (Coimbra)	7	A and B	3
250 (Villa Real)	6	Z2 and B	2 and 4
251 (Lisbon)	9	B	5
255 (Braga)	2	Z1	2

[a]In bracket a place of reference is indicated (city or region).

Table 3 Comparison of the models (*b*-value)

ZS (Zesis)	***b*-value (Share)** (Carvalho and Malfeito 2018)	***b*-value (Zesis)** (IGME 2015)	***b*-value (Ersta)** (Carvalho and Malfeito 2018)	***b*-value (EC8)** (Carvalho and Malfeito 2018)	***b*-value (mean)**[a]	***b*-value (this analysis)**
10	1.00	1.00	0.99	0.82 (0.84)[b]	0.953	0.97
13	1.00	1.06	0.75	0.77 (0.64)	0.895	0.83
7	1.00	1.06	0.88	0.86 (0.89)	0.949	1.04
6	1.00	0.98	0.94	0.82 (0.84)	0.934	0.83
9	0.90	0.87	0.79	0.71 (0.95)	0.818	0.72
2	1.00	1.04	0.98	0.66 (0.84)	0.920	0.88

[a]The mean value refers to the values of Share, Zesis, Ersta, and EC8 (except values in bracket).

[b]In bracket there are the values estimated for the same seismogenic zones and model by other authors (Sousa and Costa 2009; Sousa and Oliveira 1997; Fonseca et al. 2011).

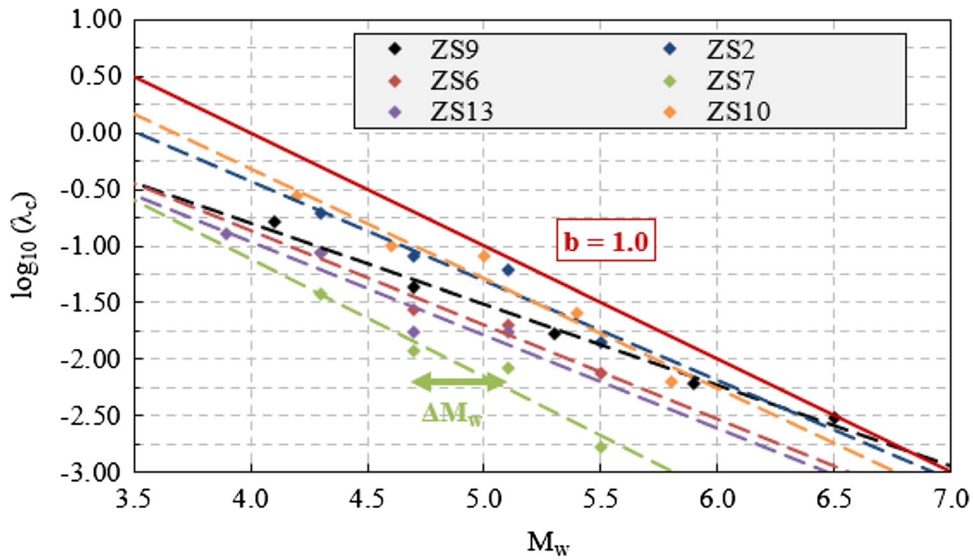

Fig. 3 G&R of this analysis for each ZS for Zesis

Table 4 Comparison of the models (*a*-value)

ZS(Zesis)	*a*-value (Share)(Carvalho and Malfeito 2018)	*a*-value (Ersta) (Carvalho and Malfeito 2018)	*a*-value (EC8) (Carvalho and Malfeito 2018)	*a*-value (mean)[a]	*a*-value (Zesis)[b]	*a*-value (this analysis)
10	3.32	2.97	2.94	3.078	3.51	3.58
13	3.00	2.27	2.56	2.610	3.41	2.35
7	3.10	3.22	2.64	2.987	3.13	3.05
6	3.60	3.45	2.94	3.328	3.31	2.48
9	3.40	3.03	2.41	2.947	2.90	2.06
2	3.30	3.56	2.64	3.167	3.80	3.09

[a]The mean value refers to the values of Share, Ersta, and EC8.

[b]Estimated value from *b*-value and G&R law.

Table 5 Comparison of the models (λ_c value)

ZS (Zesis)	λ_c (Zesis) (IGME 2015)	λ_c (this analysis)
10	0.28	0.28
13	0.13	0.13
7	0.16	0.04
6	0.19	0.09
9	0.24	0.16
2	0.32	0.19

to quantify the error only data from Zesis were available; therefore, it should be possible that it is overestimated.

Materials for the Green's function

Two main input parameters are necessary to develop the EGF, i.e., the fault and the seismic source. In a ZS, the fault is characterized by a dominant tectonic, stress regime, and main focal mechanism. The distance from the epicenter and edge of the fault rupture area is usually $\Delta < 30$ km. The source provides a list of events with a specific location, seismic moment M_0, magnitude M_w, and other parameters listed in Table 6.

The main criteria to choose the events are (i) the position of the epicenter and station must be in a ZS for Zesis, to know the seismogenic data; (ii) the epicentral depth must be $\Delta < 30$ km, to apply the PSHA; (iii) the magnitude range between $4.0 < M_w < 6.0$, to obtain significant M_0; and (iv) time-history registrations must be available, to treat the earthquake outputs.

Also, these cities are placed in a medium/high seismic hazard region with a PGA of 0.08–0.35 g in accordance with (Global earthquake model (GEM), database, Accessed in 10, 2020. Available online: https://www.globalquakemodel.org/gem).

Table 6 Used seismic events retrieved from database (Portuguese Institute of Sea and Atmosphere (IPMA) http://www.ipma.pt/pt/geofisica/sismicidade/; Luzi et al. 2016)

Datum	Event			
City	Évora	Leiria	Lisbon	Lisbon
Date, time	15/01/2018, 11:51	30/04/1999, 9:00	17/08/2017, 6:44	16/10/2000, 3:22
Latitude, longitude	38.79, – 7.93	39.82, – 8.96	39.11, – 8.92	38.70, – 9.15
ZS for Zesis (IGME 2015)	10	7	9	9
Depth, Δ (km)	11.0	22.9	12.0	20.3
M_w [a]	5.4	4.7	5.0	4.0
M_0 (N × m) [b]	1.49×10^{24}	1.39×10^{23}	3.85×10^{23}	1.30×10^{22}
Style of faulting	N/A	N/A	N/A	N/A
PGA (cm/s^2)	1.24	28.75	0.152	5.70
PGV (cm/s)	0.09	2.11	0.01	0.33
PGD (cm):	0.01	0.14	0.0	0.02
PSA_{max}	6.79	110.17	0.639	16.37
f_{max} (Hz)	1.691	1.27	1.721	2.216
f_{min} (Hz)	0.003	0.012	0.03	0.06
T_s (s)	27.24	13.66	46.04	16.61

N/A not available, *PGA* peak ground acceleration, *PGV* peak ground velocity, *PGD* peak ground displacement, PSA_{max} maximum pseudo-spectral acceleration, *f* frequency of the Fourier amplitudes, T_s significant duration (5–95% Arias intensity (Peláez et al. 2005)).

[a]Estimated values by authors as $M_w = (0.98\ M_L) + 0.58$ (Scordilis 2006; Baruah et al. 2012).

[b]Estimated values as $M_0 = 10^{(1.5\ Mw\ +\ 16.1)}$ (Hanks and Kanamori 1979).

For some events, ESM database (Luzi et al. 2016) provides a local magnitude M_L instead of M_w, which is mostly used for this type of analysis. From the literature (Scordilis 2006; Baruah et al. 2012), it is known that a unique global relation between M_L-M_w does not exist. However, a more recent relation has been calibrated (Joshi et al. 2020), in which a discrepancy of ~ 0.49 has been estimated. M_0 has been calculated in accordance with the literature (Hanks and Kanamori 1979).

The style of faulting is not available (N/A) by database. However, the reference stress regime can be taken from the respective ZSs where the event happened.

Figure 4 shows accelerograms in time, $\ddot{u}(t)$; the Fourier amplitude in function of the frequency, *f*; and the PSAs in function of structural periods, *T*. Four earthquakes have been processed by software (Seismosignal and 4.0.0, 2010) and plotted for T_s with a 5–95% Arias intensity (Peláez et al. 2005). Although they are quite "clean" recordings, the linear baseline correction and filtering with "Butterworth"-type filter and band-pass configuration (0.50–25.0 Hz) have been applied. This produces a further cleaning of the results.

Figure 5 shows the location of the epicenter (yellow star) and the station (triangle) where the PGA of each earthquake has been registered. It is possible to see that the distances are so great as to pass from a ZS to other ZS, except for the Lisbon 2000 event. The distances are (red arrow): 14.20 km (Lisbon, 2000), 181.60 km (Évora, 2018), 185.50 km (Lisbon, 2017), and 80.80 km (Leiria, 1999).

Other events have been selected to understand, in a qualitative way, seismic registration in Portugal. From these events the relations in Table 6 between M_w/M_0, M_L/M_w have been calibrated. These events, which happened in Azores islands (outside of the considered ZSs) at 10.0 km depth, are the following:

- 01/01/1980, 16:42 date; 38.81 latitude, – 27.78 longitude; 6.9 M_w; $M_0 = 2.82 \times 10^{26}$ N × m; strike-slip style of faulting.
- 27/06/1997, 4:39 date; 38.33 latitude, – 26.68 longitude; 5.9 M_w; $M_0 = 6.8 \times 10^{24}$ N × m; normal style of faulting.
- 09/07/1998, 5:19 date; 38.65 latitude, – 28.62 longitude; 6.2 M_w; $M_0 = 1.60 \times 10^{21}$ N × m; strike-slip style of faulting.
- 01/08/2000, 4:35 date; 38.79 latitude, – 29.0 longitude; 5.1 M_w; $M_0 = 5.10 \times 10^{23}$ N × m; strike-slip style of faulting.

Methodology

The proposed methodology is divided in two processes, i.e., PSHA + EGF, which are correlated to each other by M_w, that provide the pb-PSHA as shown in Fig. 6. By this methodology the first and second problem described in the "Motivation of this study" section could be overcome.

The main inputs of both models (i.e., M_w, years, M_0, M_μ) that inserted in the corresponding process (i.e., PSHA

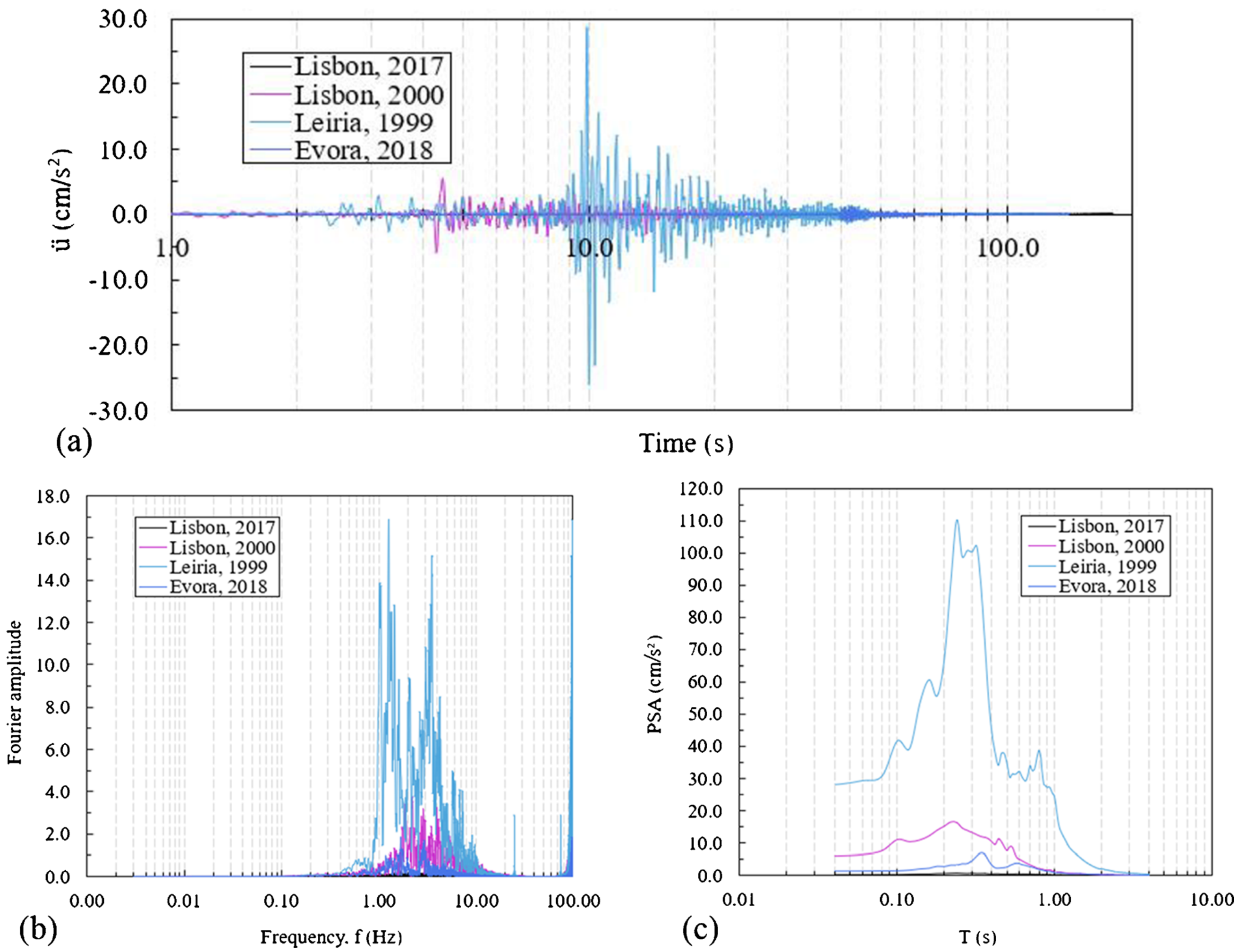

Fig. 4 Four earthquakes in terms of **a** accelerograms $\ddot{u}(t)$ in the time t, **b** Fourier amplitude vs. f, and **c** PSA vs. structural period T

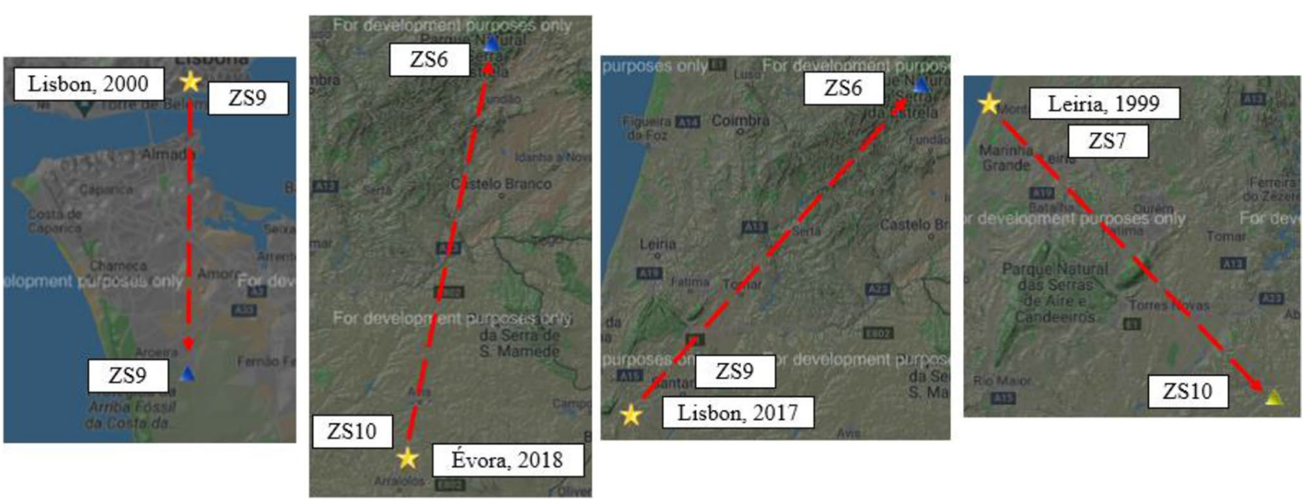

Fig. 5 Location of the epicenter (yellow star) and station (triangle) of the four earthquakes (modified from Luzi et al. (2016))

Fig. 6 General methodology for PSHA + EGF ≡ pb-PSHA

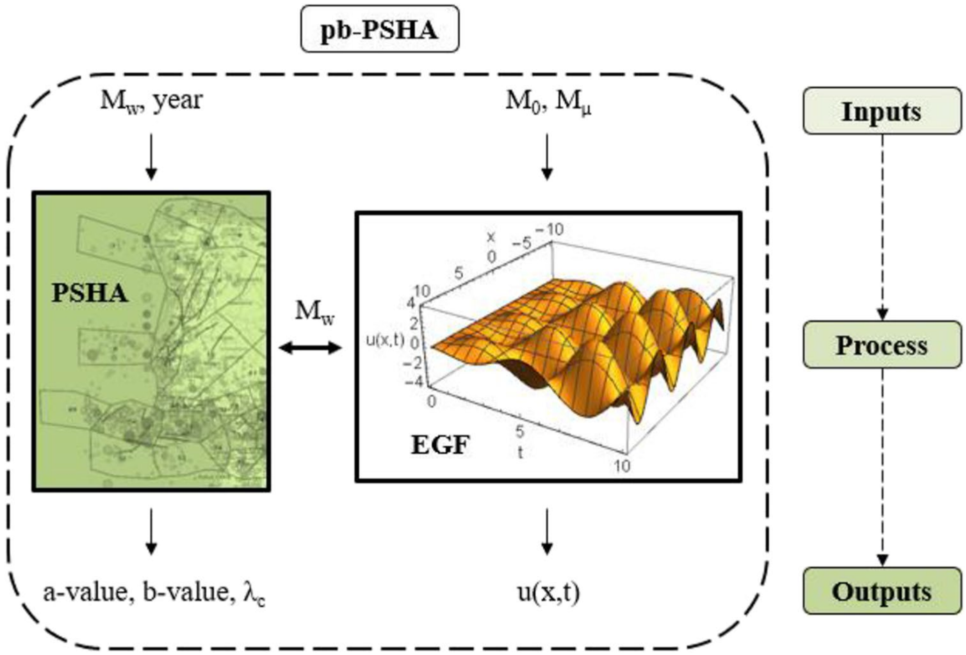

and EGF) provides the outputs (i.e., a-value, b-value, λ_c, $u(x,t)$). Both models correlate to M_w, which is treated as a probabilistic parameter in PSHA and as a physical parameter in EGF. The parameters M_μ and $u(x,t)$ will be explained in the "Empirical Green's functions" section.

Figure 7 shows the interdependencies of all parameters involved in both methods. In green are indicated the

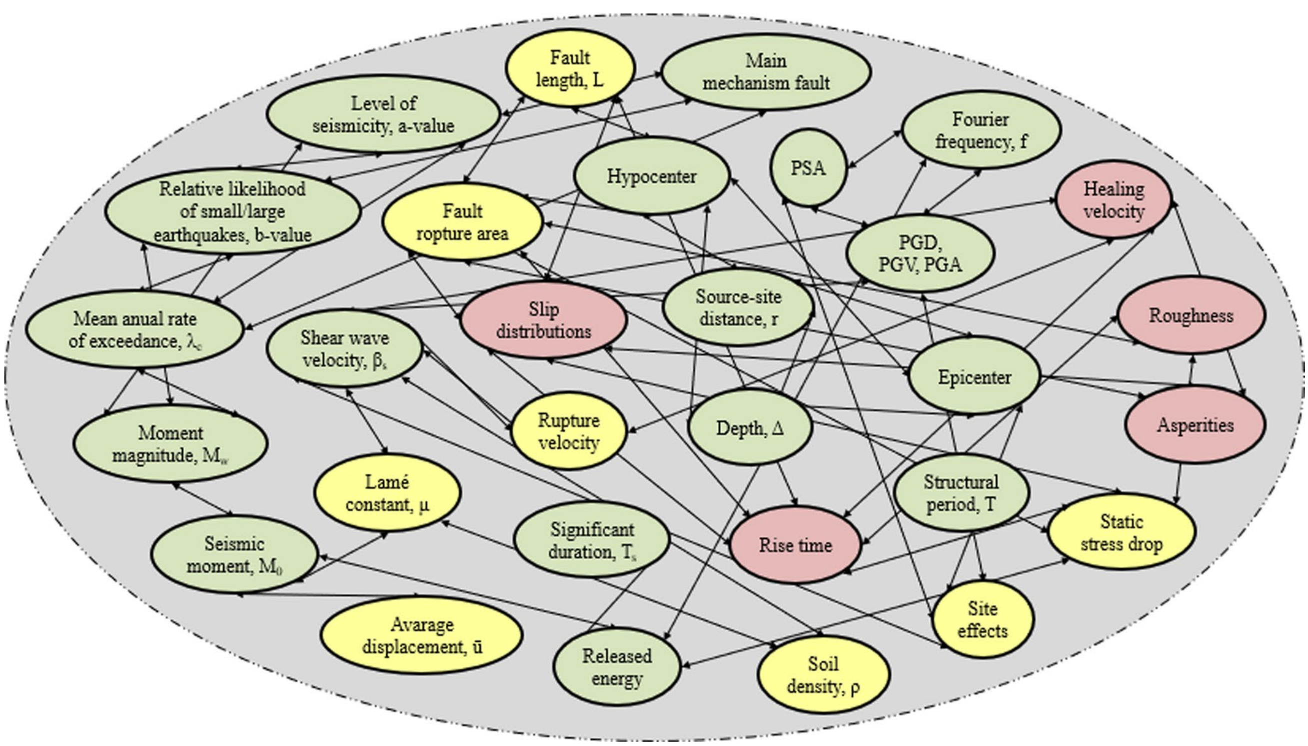

Fig. 7 Parameter interdependencies of a seismic phenomenon directly calculated (in green), indirectly calculated (in yellow), and difficult to be calculated (in red)

parameters that could be estimated in direct way by, for instance, knowing experimental or analytical relations; in yellow those parameters that could be estimated in indirect way by, for instance, knowing the event a posteriori; and in red the parameters that are very difficult to be estimated. The purpose of Fig. 7 is showing the real difficulty of predicting and controlling a seismic phenomenon. Some parameters have been treated in this paper; other ones can be retrieved in specialized literature (Hutchings et al. 1997; Sorensen et al. 2007; Jeremias et al. 2012).

Seismic hazard

The PSHA is based on the Cornell method (Cornell 1968) and the Poisson distribution (Ross 2008). A truncated exponential probability density function (PDF) at the minimum, $M_{w,\min}$, and maximum magnitude moment, $M_{w,\max}$, is used. The probability of exceedance P_e of several magnitudes, $\mu_{w,i}$, associated to a specific seismogenic zone and correlated to a PDF for source-side distance r in a range $r_{\min} \le r \le r_{\max}$, $f_R(r)$, is described by the following (Faccioli and Paolucci 2005; Valentini et al. 2019):

$$P_e\left[M_w > \mu_{w,i}\right] = \int_{r_{\min}}^{r_{\max}} P_e\left[M_w > \mu_{w,i}\right] f_R(r) dr = \int_{r_{\min}}^{r_{\max}} \left(\frac{e^{-(\beta(\mu_{w,i} - M_{w,\min})} - e^{-(\beta(M_{w,\max} - M_{w,\min})}}{1 - e^{-\beta(M_{w,\max} - M_{w,\min})}} \right) \frac{r}{L\sqrt{r^2 - \Delta^2}} dr \approx \frac{e^{-(\beta(\mu_{w,i} - M_{w,\min})} - e^{-(\beta(M_{w,\max} - M_{w,\min})}}{1 - e^{-\beta(M_{w,\max} - M_{w,\min})}} \quad (1)$$

where L is the fault length, Δ is the vertical projection of the fault at ground surface, and $\beta = b \log_e 10$. PDF of $f_R(r)$ is expressed by an equation that models a shallow fault as a linear source.

From Eq. (1) the probability of not-exceedance $P_{ne}[M_w \le \mu_{w,i}]$ and the return period $T_{\mu w,i}$ can be defined by well-known relations (Faccioli and Paolucci 2005).

Empirical Green's functions

Basic hypotheses of the model

The use of EGFs is based on the literature (Aki and Richards 2002; Stein and Wysession 2005; Hutchings 1994) where EGF only represents the medium, through the effects of propagation. EGF is a vector record that includes the seismic source. For the definition of a seismic source, events small enough are used in order that the frequency of interest is below the source corner frequency, thus that the source of the EGF is a step function, which it is removed by deconvolution. Therefore, EGF is convolved with the source function. If it is not possible to find events small enough, it is deconvolved out a Brune source (Mert et al. 2016), which works for small magnitude (<4.0), to obtain the propagation of EGF.

In this study, in a similar way, the EGF represents a vector that accounts for the contribution of wave equations, whereas the source function is defined by another function that is convoluted with the EGF. Thus, EGF is inserted directly into the elasto-dynamic equation, as detailed in the following section. In many cases, the source is at a point in space or time, so that the seismic source contains delta functions and can be easily integrated. A feature of this formulation is that the principle of reciprocity, which states that the source and the receiver can be interchanged, emerges directly (Stein and Wysession 2005).

Theoretical model

The analysis of displacement discontinuities across an internal surface Ω is treated. The aspect is to pass from a surface Ω to a line x' (see Appendix).

EGFs for a time-dependent t differential operator $\mathcal{L}(u(x, t))$ over the region Ω is defined to be a solution $g(x', t'; x, t)$ of $\mathcal{L}(g(x', t'; x, t)) = \delta(x - x')\delta(t - t')$, by the Dirac delta function δ (Aki and Richards 2002), that satisfies the given homogeneous boundary conditions $\mathcal{B}(u(x, t))$ (Aki and Richards 2002; Baker and Sutlief 2003; António and Tadeu 2002). A particular solution of $\mathcal{L}(u(x, t)) = f(x, t)$ with homogeneous boundary $\mathcal{B}(u(x, t))$ in a general medium can be obtained by performing a convolution integral:

$$\int_0^\infty dt' \int_{x' \in \Omega} f(x', t') g(x', t'; x, t) dx' \quad (2)$$

The elastic-dynamic equation of an earthquake and its ground motions is here represented. The ground displacement, $u(x, t)$, in the direction $\hat{x}_n$, at location x and time $t > 0$, is as follows (Hutchings and Viegas 2012):

$$u(x, t) = \int_{-\infty}^{\infty} \int_0^{\infty} f(x', t') g(x, t; x', t') dx' dt' \quad (3)$$

where $f(x', t')$ is a seismic source function in $\hat{x}_q$ direction, at location x' ($\equiv L$ in Eq. (1)) and time t', and $g(x, t; x', t')$ is the Green's function tensor. The Green's function tensor is the contribution to the displacement in the $\hat{x}_n$ direction from a unidirectional unit impulse in direction $\hat{x}_p$ (see Fig. 8b).

The integrals of Eq. (3) provide the total response due to the source distribution. In this case, the source is limited in the space x' and time t'. Therefore, the integral is not calculated over the source region Ω.

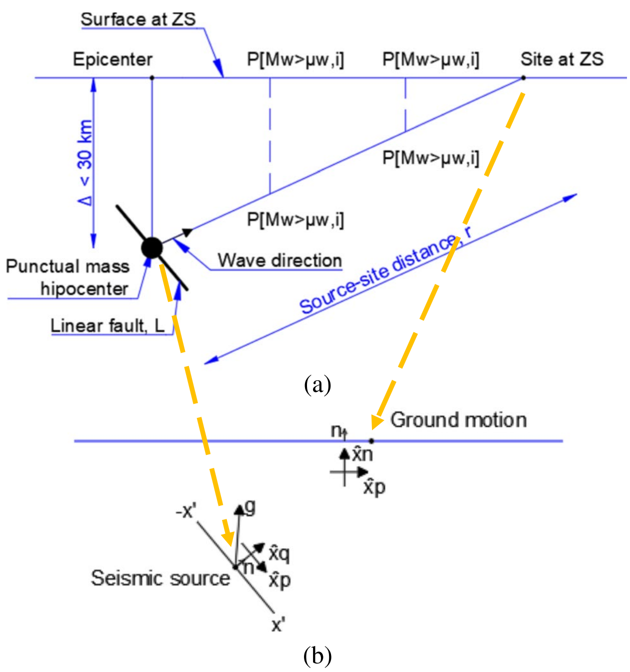

Fig. 8 Proposed model for PSHA + EGF: **a** general representation and **b** vectors and tensors at seismic source and ground motion

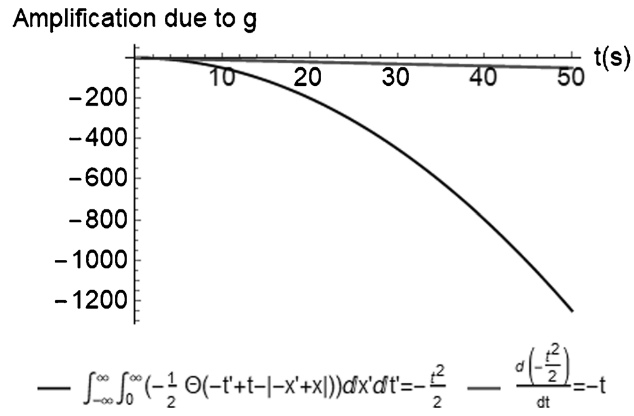

Fig. 9 Plot of Eq. (4) in Eq. (3) with $f(x', t') = 1$, integrated for $-\infty < x' < +\infty$ and $t' \geq 0$

The use of the $g(x, t; x', t')$ provides a solution for a partial differential operator $\mathcal{L}(u(x, t))$ with boundary conditions $\mathcal{B}(u(x, t))$ in the range $x_{\min}$ to $x_{\max}$, described as g:{$\mathcal{L}(u(x, t)$, $\mathcal{B}(u(x, t))$, $u(x, t)$, {x, $x_{\min}$, $x_{\max}$}, and t, {x', t'}} (Mathematica and 12, software version number 12.0, 2019). To solve the nonhomogeneous (i.e., $\neq 0$) wave equation (Kramer 1996; Vretos 2013) using g and with the solution of $\mathcal{L}(u(x, t))$ as one-dimensional x equation of transversal body waves β_s (García et al. 2016) with unbounded, $\mathcal{B} = 0$, the relation becomes $g:\{\frac{\partial^2 w(x,t)}{\partial x^2} - \frac{1}{\beta_s^2}\frac{\partial^2 w(x,t)}{\partial t^2}, \mathcal{B} = 0, w(x, t), \{x, -\infty, \infty\}, t, \{x', t'\}\}$, with $\beta_s^2 = (\mu/\rho)^{1/2} = 1$ (μ is the Lamé constant and ρ is the material density).

g solution is as follows:

$$g = -\frac{1}{2}\Theta\left[\left(-t' + t\right) - \left|-x' + x\right|\right] \tag{4}$$

where $\Theta(x, t, x', t')$ is the heaviside theta step function, which is assumed as a displacement discontinuity (Stein and Wysession 2005). Θ is a multidimensional function, which is 1 only if none of the x, t, x', and t' are not positive and $|\cdot|$ is the modulus.

Equation (4) represents the solution of the wave equation through Θ function. By substituting Eq. (4) in Eq. (3) with $f(x', t') = 1$, it is possible to plot the trend due to the amplification of the Green's function g as shown in Fig. 9.

In fact, the solution of Eq. (3) is a space and time convolution, and the spatial part is two (or three) dimensional, and that it will affect the seismograms. However, this amplification quantifies the physical nature of the seismic source; therefore, a reduction should not be necessary.

Equation (3) contains the characteristics of the source related to released energy; however, also by using Eq. (4), it does not describe the ground motion. Therefore, a further function should be introduced. The key of the problem is to define a nonhomogeneous term for $f(x', t')$ to describe the seismic source function in spatial x' and time t' distribution of slip along the fault (Hutchings 1992).

In (Ma et al. 2019a), the seismic source is idealized by using four different mechanism failures. In a similar way, here, $f(x', t')$ is represented by a following function (i.e., random, impulsive, periodic, or linear).

$$f\left(x', t'\right) = \begin{cases} \sum_{i=1}^{n} a_{h,i}\left(\sin\left(\omega_i t' + \phi_i\right) + \cos\left(\omega_i x' + \phi_i\right)\right) & \text{Random} \\ a_h \sin\left(x'\right) e^{-t'} & \text{Impulsive} \\ a_h\left(\sin\left(x'\right) + \cos\left(t'\right)\right) & \text{Periodic} \\ a_h\left(x' + t'\right) & \text{Linear} \end{cases} \tag{5}$$

where a_h is the amplitude of the source function (described in the "Hypocenter with a punctual mass" section), ω_i is the circular frequency ($\omega_i = 2\pi f_i$), ϕ_i is a random phase between 0 and 2π, and n is the number of summed simple harmonic components (here $n = 1500$).

Equation (5) is expressed by four different function types to try to simulate the characteristics of a seismic source since its accelerations are unknown (Lior and Ziv 2018), with a sine/cosine/exponential function that could represent the trend in time t' and space x'. In this sense, Eq. (5) defines a seismic source in both deterministic (impulsive, period, linear) and probabilistic (random) form.

It is important to note that, if there is consistency with a possible motion of the energy propagation, there may not be consistency with the rupture.

Hypocenter with a punctual mass

Equation (4) does not represent a physical quantity; therefore, it should be necessary to give a physical meaning to Eq. (5). As shown in literature (Hutchings and Viegas 2012), the source function can be obtained by the Lamé constant (or shear modulus) μ, which is correlated to the seismic moment by $M_0 = \mu \times A \times \bar{u}$, where A is the rupture area and $\bar{u}$ is the average displacement (Faccioli and Paolucci 2005; Dicelis et al. 2016; Ren and Zhang 2013).

In (Hutchings and Viegas 2012), Eq. (3) is expressed as the product of the EGF times an a-dimensional amplitude of M_0, obtaining an EGF with the same units of $u(x, t)$. Also, in Ma et al. 2019a the moment tensor describes the seismic source by means of equivalent forces and moments applied at the source. In an equivalent way, here it is introduced a hypocenter with an idealized punctual mass.

A new parameter is introduced in Eq. (5) to provide a physical quantity in terms of accelerations in Eq. (3). From M_0, it is obtained an equivalent relationship: $M_0 = a_h \times M_\mu \times \bar{u}$, where a_h is the acceleration at hypocenter and M_μ is called "punctual mass hypocenter," expressed in kg. In this sense M_0 continues to be expressed as a force times a displacement, i.e., as a work.

The concept to obtain this equivalent relationship is that the shear modulus μ, calculated as a shear force divided by the area on which the force acts, is calculated as a mass times acceleration. The accumulations of static stresses released by faulting (i.e., static stress drop) have been idealized as an inertial force along a infinity fault line $\{L \equiv x' | x' (-\infty, \infty)\}$. The correlation, at mathematical level, between M_w and a mass has been already introduced in other studies (Bentz et al. 2020; McGarr 1991).

Also, in this study, the fault is considered as linear to adopt, as already mentioned, (i) the PDF of $f_R(r)$ in Eq. (1) and (ii) the domain $(-\infty, \infty)$ where the variable x' was integrated in Eq. (3).

Therefore, $x' \in \Omega$ in Eq. (2) becomes an infinity line $-\infty < x' < \infty$, as shown in Eq. (3). The solution of Eq. (3) demands this infinity range, which could be justified by the fact that the considered M_0 are very large (see Table 6); thus, the source dimensions are also very large. Moreover, the relationship between M_0 and x' is quasi-linear and tends to infinity as shown in literature (Hutchings and Viegas 2012; Ji et al. 2019; Kono et al. 2020).

Therefore, the acceleration a_h can be expressed as $a_h = M_0/(M_\mu \times \bar{u}) \approx M_0/M_\mu$ since both M_0 and M_μ have a very large magnitude (e.g., order of $\sim 10^{20}$) with respect to $\bar{u}$, which has a magnitude of meters. The objective is to estimate a unique parameter M_μ and a_h knowing PGA and M_0. This is possible through the plotting of Eq. (3) from the hypocenter to the site. In this way, only two constant values are used like to the approach shown in literature (Wennerberg 1990).

The model proposed in Fig. 8 should be valid under the following main hypotheses.

1. Epicenter and site points must be placed inside of a same ZS so that all parameters retrieved from seismogenic zones are valid.
2. Hypocenter point must be at a depth $\Delta < 30$ km since ZSs are calculated up to this depth. In this way, the probability $P[M_w > \mu_{w,i}]$ at the surface is the same at any point $P[M_w > \mu_{w,i}]$ at the wave path.
3. The source geometry must be modeled as linear. In this way Eq. (1) and Eq. (3) are valid.
4. Data of an earthquake registration must be taken from a station placed at a studied ZS. Both methods are correlated by M_w, which is retrieved from a ZS and database, and then it is inserted in EGF.

The relation $a_h \approx M_0/M_\mu$ to be introduced in Eq. (5) should be valid only mathematically. In this sense, further research will be necessary to validate the proposed model physically.

A possible limitation of this method regards its extendibility to more widespread types of earthquake events. This is because the distribution of b-values is related to the focal mechanism of the event as shown in example from the Spanish coast (2001); Gulia and Wiemer 2019). For small-magnitude events or even man-made earthquakes, the focal mechanisms can be very complicated to be identified.

Analyses and results

Return periods by PSHAs

A ZS is characterized by seismic parameters (i.e., a-value, b-value, λ_c), which are obtained from a group of events that are homogeneous and independents of each other. This indicates that for the same ZS could be possible to establish a unique period, T_e, in which these seismic parameters are maintained.

The hypothesis is that the seismogenic context for each ZS will be reasonably the same since the tectonic phenomena change during very long periods. However, the seismic parameters can suffer little variations since they are very sensible to the amount of data in the database. In this sense, a unique return period, T_e, consistent to the real sequence of events accounting for the seismogenic parameters is introduced.

The idea is not to eliminate the concept of the return period but to separate it from the acceleration, as a safety factor, since, nowadays, specific studies that provide more reliable seismic inputs are available. This aspect questions the use of extremely large return periods, $T_r > 1000$ years, to merely increase a seismic acceleration. In this sense, the third problem described in the "Motivation of this study" section could be overcome.

Figure 10 shows the results in terms of M_w vs. year for three seismogenic zones (i.e., ZS7, ZS9, ZS10) where the studied events happened (see Table 6). The dashed blue line represents the moving average regarding the events. The return period, T_e, refers to the maximum return period for which the characteristics of the seismicity remain constant, whereas the return period, $T_{\mu w}$ (interval of the vertical grey lines), is calculated as $T_{\mu w} = 1/(1 - P_{ne})$ treated in Eq. (1).

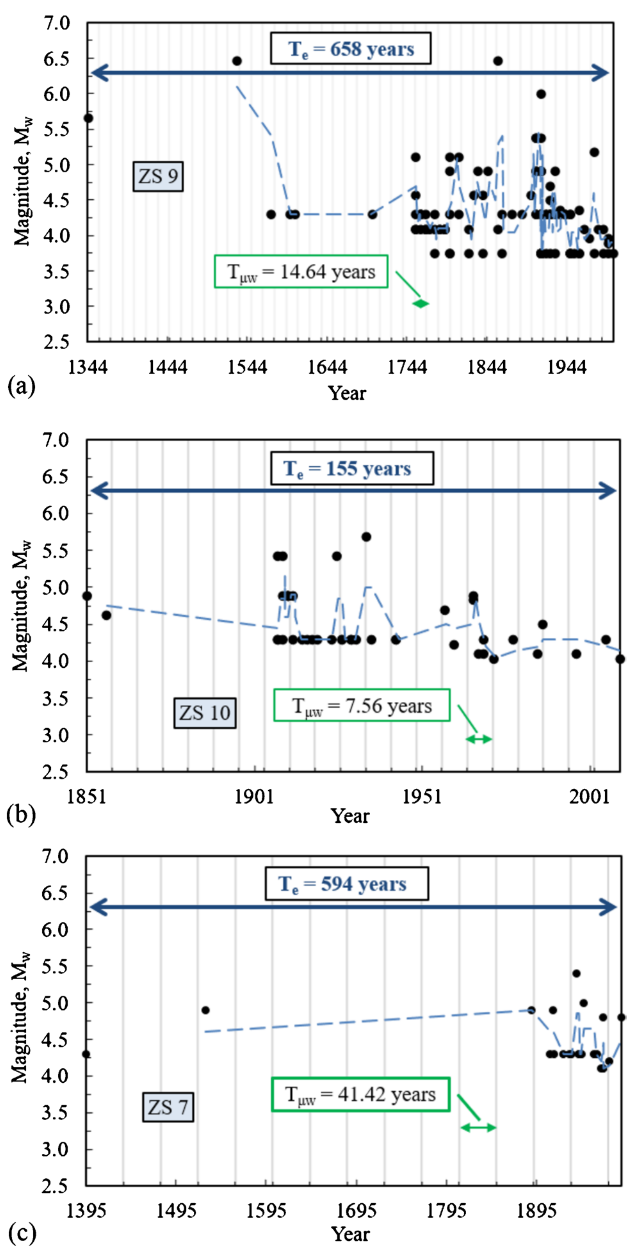

Fig. 10 Results in terms of M_w vs. year and return periods for **a** ZS9, **b** ZS10, and **c** ZS7

In Fig. 10a there are 107 events in a period 1344–2002 years with a mean magnitude of 4.3. It is possible to see that in a period 1760–2002 years the sequence of the events is more consistent to the calculated $T_{\mu w}$ (= 14.64 years); in fact, in this interval the moving average (dashed blue line) oscillates more.

Although many old events have not been recorded, these 107 events were sufficient to establish the ZS9; therefore, $T_{\mu w}$ can be assumed valid for all period of 658.0 years. These considerations are also valid for Fig. 10b, c.

Under these considerations, if $T_{\mu w} < T_r < T_e$, it is possible to assume T_r provided by Eurocode (Committee and for Standardization (CEN), Design of structures for earthquake resistance, Part 1: General rules, seismic actions and rules for buildings, 2004) ($T_r = 475$ years) for any type of structures, since this period is rightly framed in a same seismogenic context. If this range is not verified, i.e., $T_r > T_e$, a value of $T_r > 475$ years would lose meaning.

In this way, the importance factor is $\gamma_I = 1.0$. It is defined as $\gamma_I \approx (T_r/T_L)^{-1/k}$, where T_L is the return period of a requirement specific level and k is a factor that depends on the seismicity, as mentioned $k \approx 3.0$ as the a-values (see Table 4) (Committee and for Standardization (CEN), Design of structures for earthquake resistance, Part 1: General rules, seismic actions and rules for buildings 2004; Sousa et al. 2019).

It is possible to conclude, as shown in Table 7, that for these three ZSs a T_r that should be used for all type of structures, independently of their importance, is 475 years.

The results for Lisbon are consistent with the literature (Sousa and Costa 2009) where the probability of exceedance of 475 years is less than 1% for the magnitude 3.5–6.5. This could confirm that using a period longer than 475 years overestimates the seismic input by using Eurocode (Committee and for Standardization (CEN), Design of structures for earthquake resistance, Part 1: General rules, seismic actions and rules for buildings, 2004).

It is important to note that the offshore seismicity has not been considered in this study, which could affect the seismicity of the studied places as shown in literature (Sousa and Costa 2009). This is because by considering the offshore zones, e.g., ZS50, where the great 1755 Lisbon earthquake was generated, the seismicity increases as commented in

Table 7 Summary of results

Event	ZS	μ_w	$T_{\mu w}$ (year)	T_e (year)	$T_{r,\max}$ (year)
Évora, 2018	10	4.3	7.56	155.0	475.0[a]
Leiria, 1999	7	4.3	41.42	594.0	
Lisbon, 2000	9	4.3	14.64	658.0	
Lisbon, 2017					

[a]It represents the maximum T_r that could be adopted for designing of any type of structure placed in these specific ZSs.

Fonseca et al. (2011). However, as discussed in the "Motivation of this study" section, there are no attenuation equations for Portugal that can well calibrate the results at these distances (see Table 1).

These results could separate the PGA from γ_I, which relates to the consequences of a structural failure. Buildings are classified in classes, depending on the consequences of collapse for human life, public safety, civil protection, and thus social and economic consequences in the post-earthquake period (Ministerio delle Infrastructure 2008; Committee and for Standardization (CEN), Design of structures for earthquake resistance, Part 1: General rules, seismic actions and rules for buildings, 2004; Global earthquake model (GEM), database, Accessed in 10, 2020. Available online: https://www.globalquakemodel.org/gem).

The logic to divide the performance requirements in no-collapse and damage is fundamental, but it should not merely induce an increase in seismic input. It should be associated with improving mathematical modeling, seismic analyses (object of this study), design, and detailing of primary/secondary elements and connections.

An overestimation of γ_I leads to an overdesigning of, for instance, small structures considered as important since their design inertial force can reach very high values. Moreover, in many cases, the lack of attention for designing of small/medium structures makes using a high input value quickly "solve," but not totally correct, the safety problem. For this reason, it could be useful to separate the accelerations from γ_I but focusing more on the modeling and detailing.

Ground motions by EGFs

Figure 11 shows the 2D and 3D source function $f(x', t')$ for four cases (Eq. (5)): random, impulsive, periodic, and linear. The 2D trend (f vs. t') is the transversal section of the 3D trend at $x' = 0$, except for the impulsive function that is calculated at $x' = 1.5$ m. Used data refer to the Lisbon 2000 event. The numerical analyses have been carried out by Mathematica software (Mathematica and 12, software version number 12.0, 2019).

The source function, expressed by four types of functions, should represent an artificial acceleration (Zacchei and Molina 2018) of the soil at hypocenter. These functions are plotted in the significant duration T_s, i.e., $0 \leq t' \leq T_s$ (see Table 6), whereas the spatial variable x' is plotted between $-10 \leq x' \leq 10$ m.

In 3D view it is possible to see that the released energy comes from a line where the acceleration assumes a value of $f > 0$ at $t' = 0$ consistent to the proposed model.

Figure 12 shows the results for the Lisbon 2000 event in terms of displacements of the ground motion computed by using Eq. (3), which derived in the time t provides the velocities and accelerations of the ground motion.

The impulsive source function is used as reference since the parameters M_μ and a_h have been calibrated considering $(\ddot{u}(x,t) - \text{PGA}) \approx 0$ under an impulsive source function as shown also in Denolle et al. (2018). This is because an impulsive function should be consistent to the physical process described in Eq. (3) due to $\hat{x}_p$. Therefore, the amplitude a_h is calculated iteratively from registered PGA and M_0 for each event. In function of this calibration, other values of $\ddot{u}(x,t)$ are also estimated; thus, it is possible to note what the source function should well estimate $\ddot{u}(x,t)$ values.

During the time integrations, the values of the ground displacements assume larger values due to the strong influence of the Green's function, g, expressed in Eq. (4), that provides exponential values (see black line in Fig. 9).

This function mainly affects the source expressed by Eq. (5) in the displacements of the ground, whereas in the velocities and accelerations, it is possible to see that the results follow the trend of the artificial accelerograms since the influence of the Green's function is weaker.

Figures 13, 14, and 15 show the ground accelerations for the other three considered events. In general, it is possible to associate calculation results with spatial coordinates since each city has its own latitude and longitude thus seismogenic parameters.

In Table 8 there are the values of the parameters used for this analysis (i.e., a_h and M_μ).

Figure 16 shows the relative error expressed in percentage (%) calculated as (calculated value − registered value)/calculated value. The registered values are shown in Table 6. In this way it could be possible to estimate the contribution of the different source functions for PGD, PGV, and PGA.

In Fig. 16 it is possible to see that for the PGD and PGV values it is difficult to obtain a good result due to the amplification already mentioned in Fig. 9. In fact, the proposed model should estimate only the PGA values since the amplitude a_h in Eq. (5) was introduced for this scope.

For the PGA, it is possible to see that the source function expressed by a random and periodic function provides good results (i.e., non-high relative error). In particular, the periodic function provides the best results with a mean relative error for PGA of ~ 21%.

Due to the stochastic nature of the phenomenon, in some case also a random function could provide good results (see Fig. 16a). By using a linear function, the PGA values are poor, however, in some cases, provide similar values with respect the literature, e.g., for Lisbon 2000 0.15 g vs. 0.228 g (Global earthquake model (GEM), database, Accessed in 10, 2020. Available online: https://www.globalquakemodel.org/gem) and for Evora 2018 0.04 g vs. 0.08 g (Global earthquake model (GEM), database, Accessed in 10, 2020. Available online: https://www.globalquakemodel.org/gem).

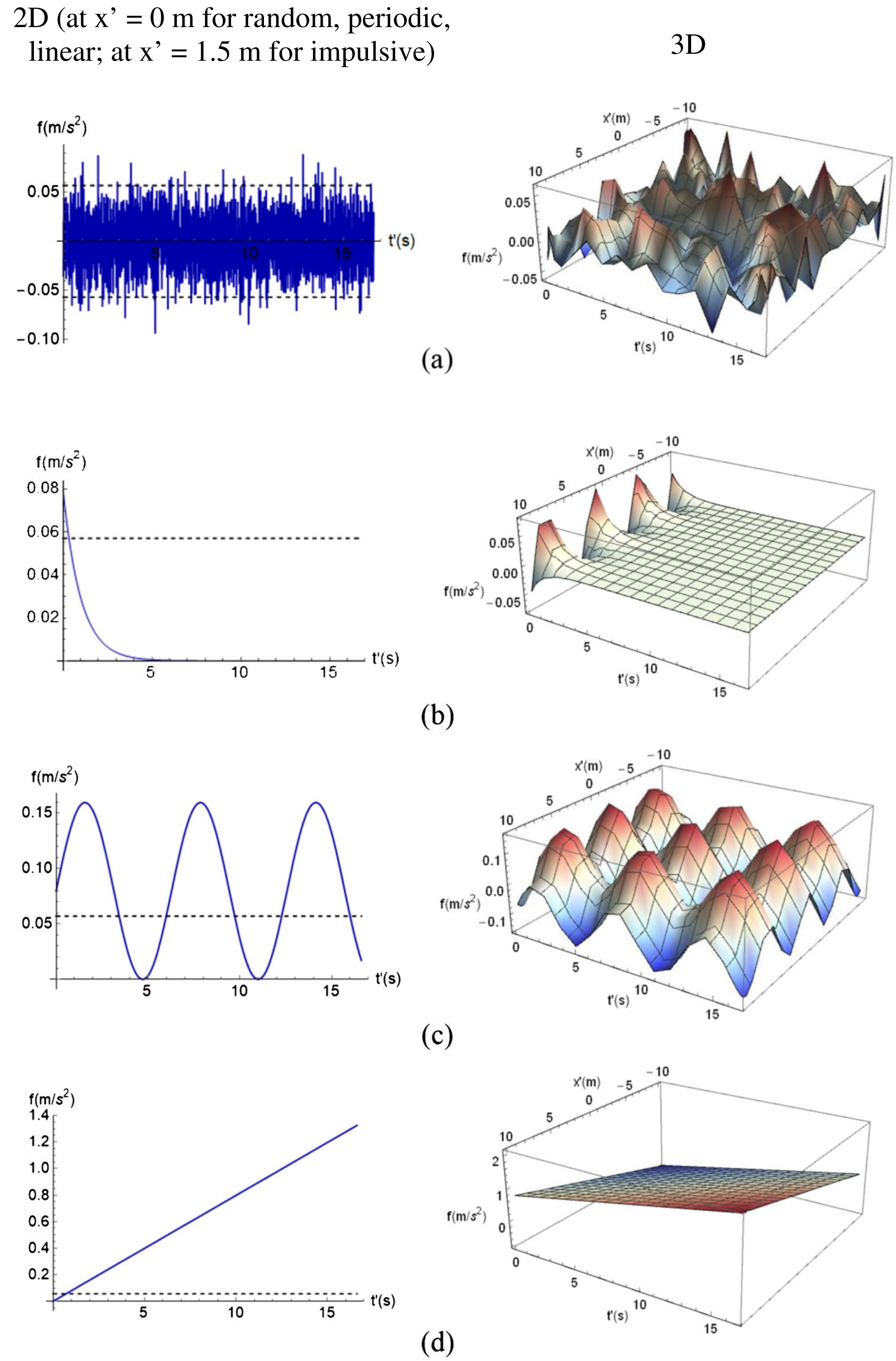

Fig. 11 2D/3D source functions expressed by a **a** random, **b** impulsive, **c** periodic, and **d** linear function. Used data refer to Lisbon 2000 event. The horizontal dashed lines in 2D functions represent the PGA value, i.e., 0.057 m/s^2 (see Table 6).

The latter aspect could be correlated to the fact that the released energy, M_0, of both events is high; therefore, a linear propagation of the seismic source function in $\hat{x}_q$ direction should not be affected by soil damping during the wave path providing high values (Denolle et al. 2018).

It is important to highlight that a station that registers the signals could be very distance to the epicenter. In many cases, this distance is larger than an equivalent radius of a ZS, and, therefore, the relation between the parameters of the PSHA and the parameters of the seismic source would not be compatible in accordance with the hypotheses of the proposed model ("Hypocenter with a punctual mass" section).

Thus, the proposed model (Fig. 8) should be applied in an area that corresponds to a unique ZS. Therefore, as

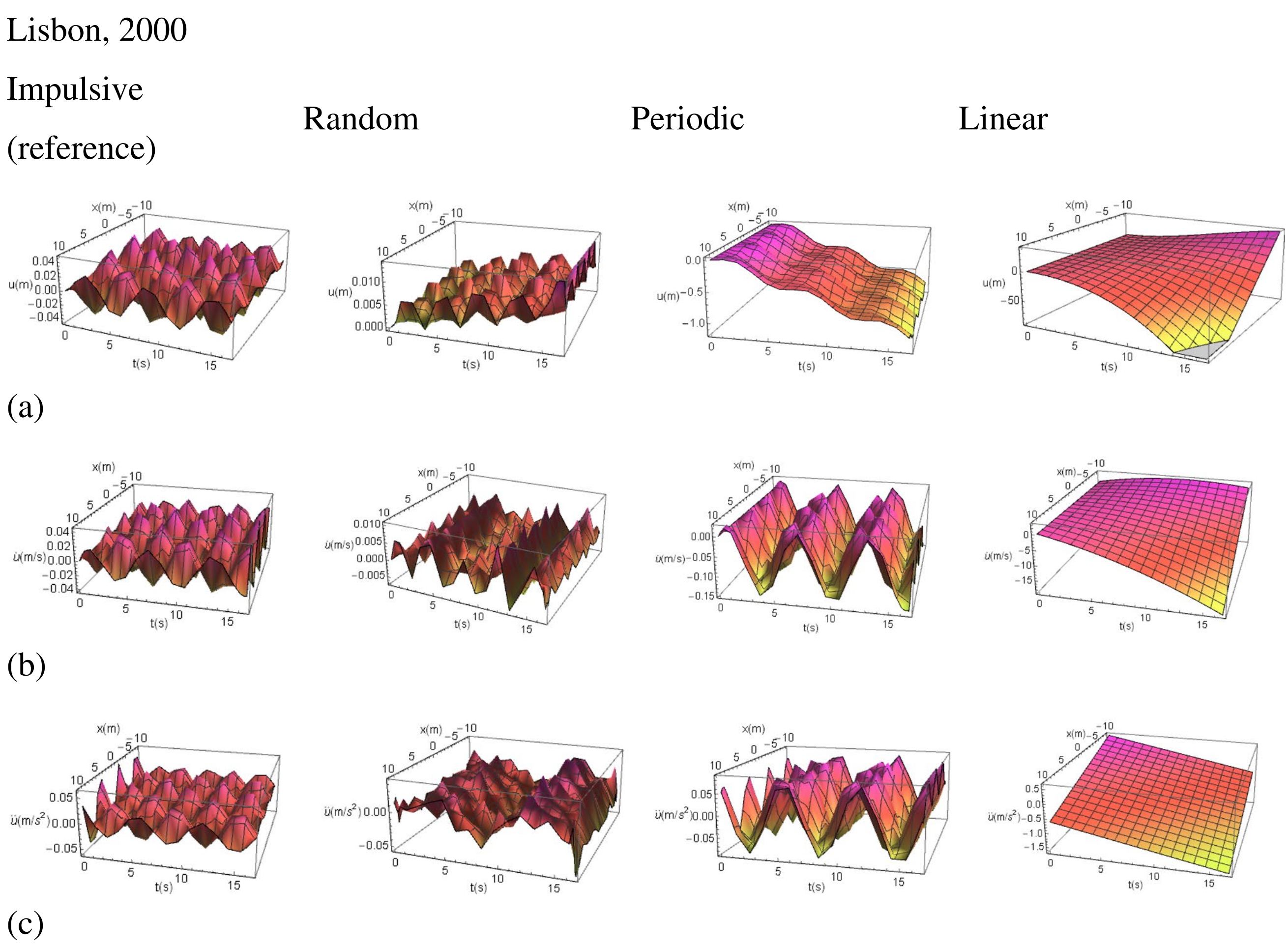

Fig. 12 Solutions in terms of **a** displacements, **b** velocities, and **c** accelerations of the ground motion for 2000 Lisbon earthquake

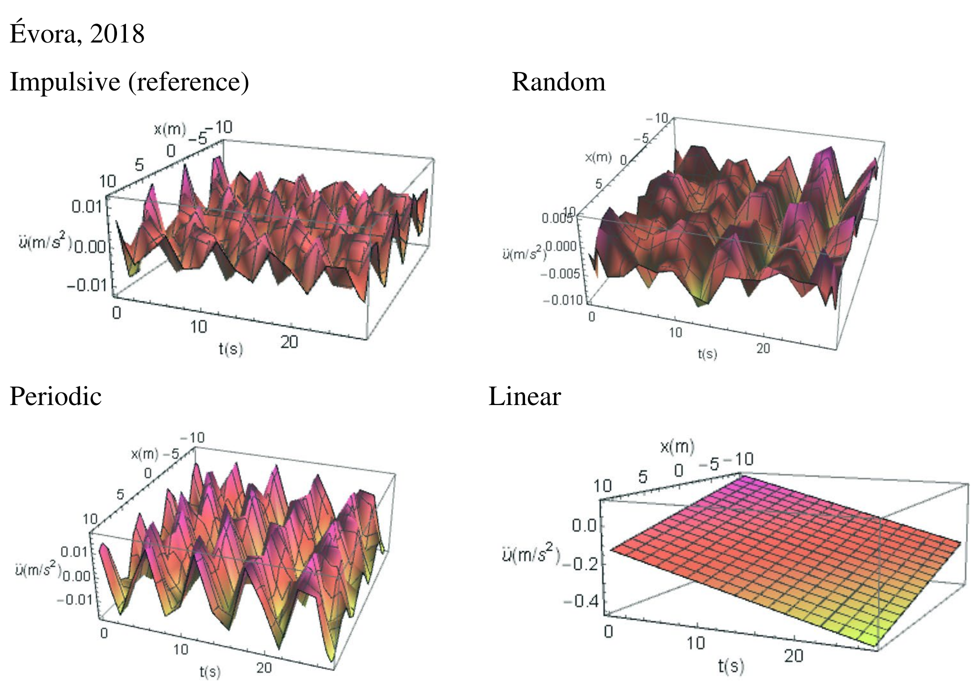

Fig. 13 Solutions in terms of accelerations of the ground motion for 2018 Évora earthquake

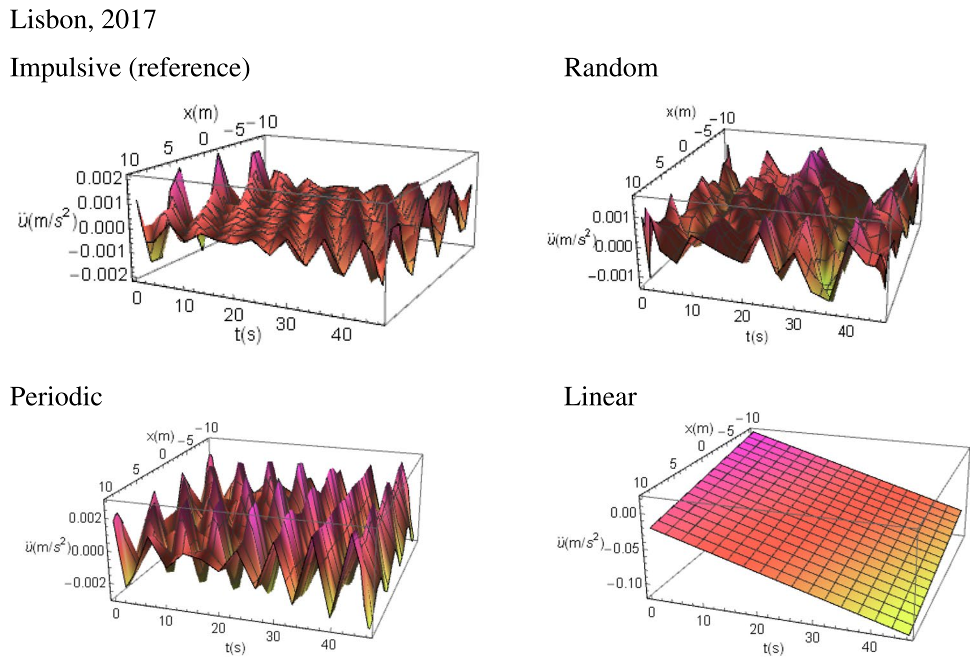

Fig. 14 Solutions in terms of accelerations of the ground motion for 2017 Lisbon earthquake

Table 8 Estimation of a_h and M_μ

	Évora, 2018	Leiria, 1999	Lisbon, 2000	Lisbon, 2017
a_h (m/s^2)	0.0124	0.276	0.0627	0.0021
M_μ (kg)	1.20×10^{23}	5.03×10^{23}	2.07×10^{23}	1.81×10^{26}

shown in Fig. 5, rigorously only the results of the 2000 Lisbon earthquake (Fig. 12) would be valid. However, mathematically, the method would continue to be also valid for other events.

This problem also exists for the traditional PSHA by using attenuation equations. In fact, when more ZSs are considered to develop a unique seismic hazard analysis, the mean parameters of ZSs are usually used. In this way, the mean of *b*-values for several ZSs are calculated in the detriment of the adopted attenuation equation which is usually calibrated for a unique predominant and homogenous mechanism fault (Zacchei et al. 2017).

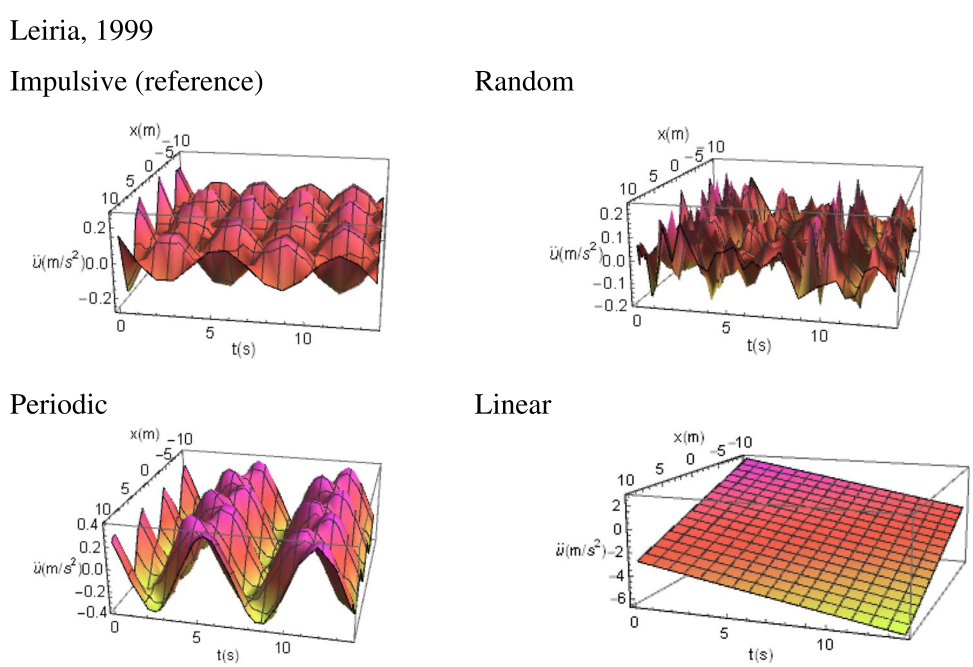

Fig. 15 Solutions in terms of accelerations of the ground motion for 1999 Leiria earthquake

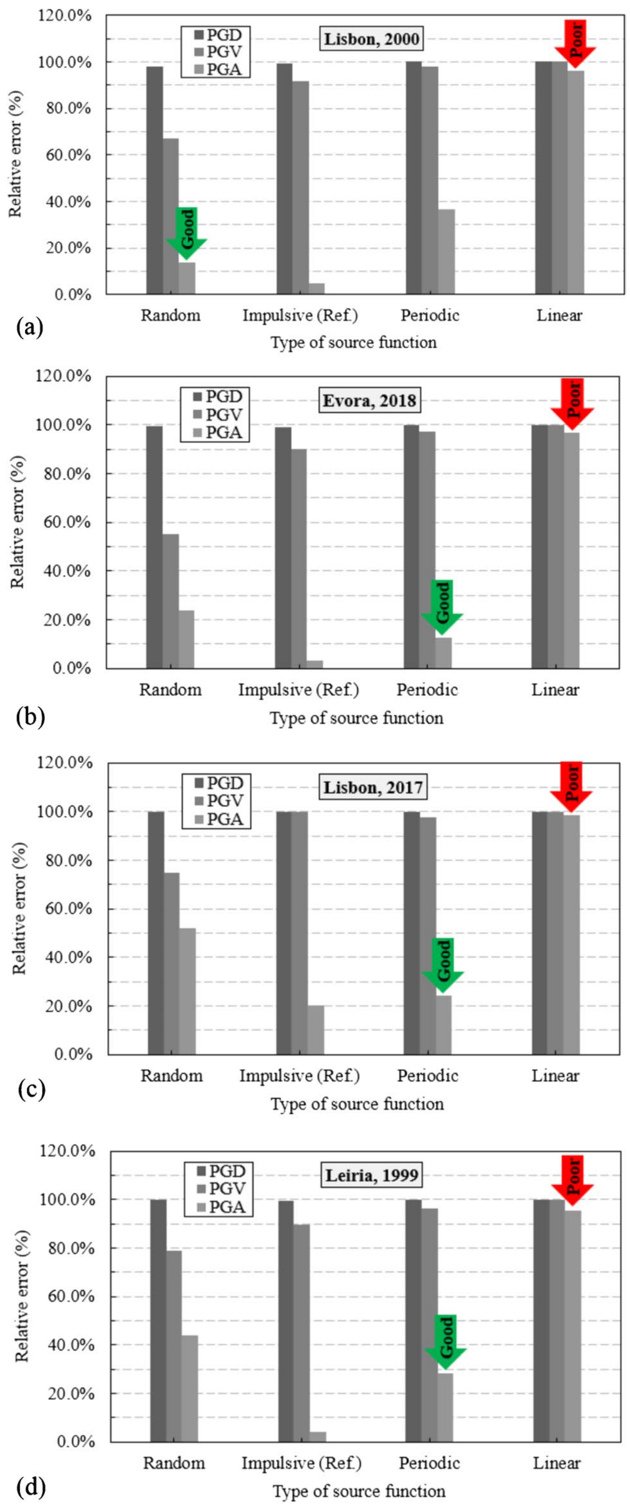

Fig. 16 Relative error of the source functions for the **a** 2000 Lisbon, **b** 2018 Evora, **c** 2017 Lisbon, and **d** 1999 Leiria event

Conclusions

This paper combines the PSHA with EGFs through a magnitude M_w describing the source function via random, impulsive, periodic, and linear functions. Some parameters of ZSs for Portugal and specific return periods have been estimated.

The main conclusions are the following:

1. A comparison between the parameters of existing seismogenic zones (Share, Ersta, EC8, Zesis) and other estimated parameters has been carried out. Results listed in Tables 3, 4, and 5 show some differences by using same ZSs and models indicating that the epistemic uncertainties play an important role. The results in this paper could contribute to reduce the gap from various models.
2. An overestimation of γ_I leads to an overdesigning of, for instance, small structures considered as important, since the design inertial force can reach very high values with a small increasing of γ_I. In many cases, for small/medium structures, the use of a high input value "resolves" the safety problem neglecting an attention for designing. For this reason, it could be convenient to separate the PGA from γ_I as shown in Table 7. For important small structures it should be essential focusing more on the modeling and detailing.
3. A new model to correlate PSHA with EGFs has been proposed (Fig. 8). This model should be valid under specific hypotheses. It has been calibrated for Portugal; however, more research are necessary to validate it experimentally. The key parameter for the correlation between two models is M_w, which is estimated by PSHA and introduced in EGFs by M_0 through the following relation: $a_h \approx M_0/M_\mu$.
4. Different types of source functions have been used to carry out the proposed model: random, impulsive, periodic, and linear. This is because a priori the accelerations of the seismic source are not known. Results (Fig. 16) show that the periodic function provides better results with a relative error between 12 and 36%. These results could be of importance for hazard assessment to incentivize more further research on the earthquake source physics in general.

Appendix

The inhomogeneous (i.e., $\neq 0$) wave equation in one dimension for a function $w(x, t)$ is, for $-\infty < x < \infty$, $t > 0$, given by the following (the process was retrieved from Baker and Sutlief (2003) and adapted to this study):

$$\frac{\partial^2 w(x,t)}{\partial x^2} - \frac{1}{\beta_s{}^2}\frac{\partial^2 w(x,t)}{\partial t^2} = h(x,t) \tag{A1}$$

for some given function $h(x, t)$.

The Green's function $g(x, t; x', t')$, by the Dirac delta function δ (Aki and Richards 2002), associated with Eq. (A1) satisfies

$$\frac{\partial^2 g(x,t;x',t')}{\partial x^2} - \frac{1}{\beta_s^{\,2}}\frac{\partial^2 g(x,t;x',t')}{\partial t^2} = \delta(x-x')\delta(t-t') \quad (A2)$$

By using a Fourier's transform, it is obtained:

$$\frac{1}{\beta_s^{\,2}}\frac{\partial^2 G(x,t;x',t')}{\partial t^2} + x^2 G(x,t;x',t') = \delta(t-t')e^{ixx'} \quad (A3)$$

Let $G(x, t; x', t') = \exp(ixx')\, r(x, t)$, a function $r(x,t)$,

$$\frac{1}{\beta_s^{\,2}}\frac{\partial^2 r(x,t)}{\partial t^2} + x^2 r(x,t) = \delta(t-t') \quad (A4)$$

therefore

$$\frac{1}{\beta_s^{\,2}}\frac{\partial^2 r(x,t)}{\partial (t-t')^2} = -x^2 r(x,t) \quad (A5)$$

which has solutions $r(x, t) = A(t)\sin[x(t-t')]$, with $A(t) = \int \delta(t-t')/x\, dt$, is an amplitude of sine function.

By using the fact that $\int \delta(t-t')dt = \Theta(t-t')$, $r(x, t)$ is

$$r(x,t) = \frac{\sin[x(t-t')]\Theta(t-t')}{x} \quad (A6)$$

therefore, considering the equivalence between Eq. (A3) and Eq. (A4),

$$G(x,t;x',t') = \frac{e^{ixx'}\sin[x(t-t')]\Theta(t-t')}{x} \quad (A7)$$

Thus, it is shown that the Fourier's transform in x of the Green's function, $G(x, t; x', t') = F(g(x, t; x', t'))$, is given by Eq. (A7).

Finally, by taking the inverse of Fourier's transform

$$g(x,t;x',t') = F^{-1}[G(x,t;x',t')] = \frac{1}{2\pi} = \int_{-\infty}^{\infty} G(x,t;x',t')e^{-ix^2}dx = \int_{-\infty}^{\infty} \frac{\Theta(t-t')sin[x(t-t')]e^{ix(x'-x)}}{2\pi x}dx \quad (A8)$$

and by using two general identities (i) $2\sin(\alpha)(\cos(\beta) + \sin(\beta)) = \sin(\alpha-\beta) + \sin(\alpha+\beta) + \cos(\alpha-\beta) - \cos(\alpha+\beta)$ and (ii) $e^{i\alpha} = \cos(\alpha) + i\ \mathrm{sen}(\alpha)$, it is obtained.

$$g(x,t;x',t') = \frac{\Theta(t-t')}{4\pi}\int_{-\infty}^{\infty}\left(\frac{sin[x(t-t'+x'-x)]}{x} + \frac{sin[x(t-t'-x'+x)]}{x} + i\frac{cos[x(t-t'+x'-x)]}{x} + i\frac{cos[x(t-t'-x'+x)]}{x}\right)dx \quad (A9)$$

Neglecting the imaginary part, knowing that $\int_{-\infty}^{\infty}\frac{\sin(\alpha)}{\alpha}d\alpha = \pi$ and introducing the sign function as $\mathrm{sgn}(\alpha) = -1, 0, 1$ for $\alpha < 0$, $\alpha = 0$, $\alpha > 0$, respectively, Eq. (A9) is

$$g(x,t;x',t') = \frac{\Theta(t-t')}{4\pi}\pi(\mathrm{sgn}(t-t'+x'-x) + \mathrm{sgn}(t-t'-x'+x)) \quad (A10)$$

that, considering $\mathrm{sgn}(\alpha) \approx 2\,\Theta(\alpha)$, can be written as

$$g(x,t;x',t') = -\frac{1}{2}\Theta[(-t'+t) - |-x'+x|)] \quad (A11)$$

that is Eq. (4).

Note that Eq. (4) has a similar form with respect to the general solution of Eq. (A1) with $h(x.t) = 0$, $\beta_s = 1$, and unbounded condition $B = 0$, that is, $w(x, t) = c_1(t-x) + c_2(t+x)$, where c_1 and c_2 are two arbitrary differential equations.

Funding The first author received support from the Itecons Institute, Coimbra, Portugal, for the Wolfram Mathematica license, and University of Coimbra (UC), Portugal, to pay authorship dues (when applicable) to completely download all papers in references. The second author received support from CNPq and FAPESP, both Brazilian research funding agencies.

Declarations

Conflict of interest The authors declare no competing interests.

References

Ahulu ST, Danuor SK, Asiedu DK (2018) Probabilistic seismic hazard assessment of southern part of Ghana. J Seismol 22:539–557

Aki K, Richards PG,(2002) Quantitative seismology, Ed. Jane Ellis, 2 ed,743

Ambraseys NN, Douglas J, Sarma SK, Smit PM (2005) Equations for the estimation of strong ground motions from shallow crustal earthquakes using data from Europe and the Middle East:

horizontal peak ground acceleration and spectral acceleration. Bull Earthq Eng 3:1–53

Ansary MA, Arefin MR (2020) Assessment of predominant frequencies in Dhaka city, Bangladesh using ambient vibration, Asian. J Civ Eng 21:91–104

António J, Tadeu A (2002) 3D seismic response of a limited valley via BEM using 2.5D analytical Green's functions for an infinite free-rigid layer. Soil Dyn Earthq Eng 22:659–673

Baker M, Sutlief S (2003) Green's functions in physics, Version 1, p. 332, Seattle, Washington, U.S

Barone G, Lo Iacono F, Navarra G, Palmeri A (2015) A novel analytical model of power spectral density function coherent with earthquake response spectra. In: 1st ECCOMAS Thematic Conference on Uncertainty Quantification in Computational Sciences and Engineering, Crete island, Greece, pp 25–27 May 2015.

Baruah S, Baruah S, Bora PK, Duarah R, Kalita A, Biswas R, Gogoi N, Kayal JR (2012) Moment magnitude (M_w) and local magnitude (M_L) relationship for earthquakes in Northeast India. Pure Appl Geophys 169:1977–1988

Bentz S, Kwiatek G, Martínez-Garzón P, Bohnhoff M, Dresen G (2020) Seismic moment evolution during hydraulic stimulations. Geophys Res Lett 47:1–9

Carvalho A (2007) Modelação Estocástica da Acçao Sísmica em Portugal Continental, PhD Thesis, University of Lisbon, Portugal, p 392

Carvalho J, Dias R, Ghose R, Teves-Costa P, Borges J, Narciso J, Pinto C, Leote J (2018) Near-surface characterization of the Lisbon and Lower Tagus Valley area, Portugal, for seismic hazard assessment: VS30 and soil classification maps. Bulleting of the Seismological Society of America 108:2854–2876

Carvalho A, Malfeito N (2018) Mapas de Perigosidade Sismica para Portugal Continental: Uma Analise Critica, Parte I – Periodos de recorrencia de sismos, Technical report 363/2018 – DE/NESDESPES, Lisbon, Portugal.

Chan CH, Wu YM, Cheng CT, Lin PS, Wu YC (2013) Scenario for a short-term probabilistic seismic hazard assessment (PSHA) in Chiayi, Taiwan. Terr Atmos Ocean Sci 24:671–683

Clough RW, Penzien J (2003) Dynamics of structures, 3rd edn. McGraw-Hill, New York, USA, p 752

Cornell CA (1968) Engineering seismic risk analysis. Bull Seism Soc Ame 58:1583–1606

Cunha TA, Matias LM, Terrinha P, Negredo AM, Rosas F, Fernandes RMS, Pinheiro LM (2012) Neotectonics of the SW Iberia margin, Gulf of Cadiz and Alboran Sea: a reassessment including recent structural, seismic and geodetic data. Geophys J Int 188:850–872

Denolle MA, Boué P, Hirata N, Beroza GC (2018) String shaking predicted in Tokyo from an expected M7+ Itoigawa-Shizuoka earthquake. J Geophys Res Solid Earth 123:3968–3992

Dicelis G, Assumpção M, Kellogg J, Pedraza P, Dias F (2016) estimating the 2008 Quetame (Colombia) earthquake source parameters from seismic data and InSAR measurements. J S Am Earth Sci 72:250–265

Dong L, Shu W, Sun D, Li X, Lingyun Z (2017) Pre-alarm system based on real-time monitoring and numerical simulation using internet of things and cloud computing for tailings dam in mines. IEEE Access 5:1–10

Douglas J (2019) Ground motion prediction equations 1964–2019, Database, 2019. Link: http://www.gmpe.org.uk/gmpereport2014.html. Accessed October 2020

European Committee for Standardization (CEN) (2004) Design of structures for earthquake resistance, Part 1: General rules, seismic actions and rules for buildings, BS EN 1998–1:2004, Brussels, Belgium.

Faccioli E, Paolucci R (2005) Elementi di sismologia applicata all'ingeneria. Pitagora Editrice, Bologna, Italy.

Fergany E, Hutchings L (2017) Demonstration of pb-PSHA with Ras-Elhekma earthquake. Egypt NRIAG J Astr Geoph 6:41–51. https://doi.org/10.1016/j.nrjag.2017.03.002

Fonseca JFBD, Vilanova SP, Comment on Sousa ML and Costa AC (2011) Ground motion scenarios consistent with probabilistic seismic hazard disaggregation analysis, Bull. Earthquake Eng, 9:1289–1295

García F, Aznárez JJ, Padrón LA, Maeso O (2016) Relevance of the incidence angle of the seismic waves on the dynamic response of ach dams. Soil Dyn Earthq Eng 90:442–453

García-Pérez J, Castellanos F, Díaz O (2005) Occupancy importance factor in earthquake engineering. Eng Struct 27:1625–1632

Global earthquake model (GEM), database, Accessed in 10/2020. Available online: https://www.globalquakemodel.org/gem.

Gràcia E, Dañobeita J, Vergés J (2003) Mapping active faults offshore Portugal (36°N–38°N): implications for seismic hazard assessment along the southwest Iberian margin. Geology 31:83–86

Gulia L, Wiemer S (2019) Real-time discrimination of earthquake foreshocks and aftershocks. Nature 574:193–200

Gutscher MA, Baptista MA, Miranda JM (2006) The Gibraltar Arc seismogenic zone (part 2): constraints on a shallow east dipping fault plane source for the 1755 Lisbon earthquake provided by tsunami modelling and seismic intensity. Tectonophysics 426:153–166

Ministério da Habilitação, Obras Públicas e Transportes, Regulamento de Solicitações em Edifícios e Pontes (RSA), I Serie, No. 125, 1-05-1983, Lisbon, Portugal p. 34.

Hanks TC, Kanamori H (1979) A moment magnitude scale. J Geophys Res 84:2348–2350

Hariri-Ardebili MA, Saouma VE (2016) Seismic fragility analysis of concrete dams: a state-of-the-art review. Eng Struct 128:374–399

Hutching L, Mert A, Fahjan Y, Novikova T, Golara A, Miah M, Fergany E, Foxall W (2017) Physics-based hazard assessment for critical structures near large earthquake sources. Pure Appl Geophys 174:3635–3662

Hutchings L (1992) Modeling earthquake ground motion with an earthquake simulation program (EMPSYN) that utilizes empirical Green's functions, Technical Report UCRL-ID-105890, 119.

Hutchings L (1994) Kinematic earthquake models and synthesized ground motion using empirical Green's functions. Bull Seismol Soc Am 84:1028–1050

Hutchings L, Viegas G (2012) Application of empirical Green's functions in earthquake source, wave propagation and strong ground motion studies. Earthq Res Anal – New Front Seismol, InTech, Sect 3:87–140

Hutchings L, Stavrakakis GN, Ioannidou E, Wu FT, Jarpe S, Kasameyer P (1997) Strong ground motion synthesis for a M = 7.2 earthquake in the Gulf of Corinth, Greece using empirical Green's functions, 29th IASPEI General Assembly, Thessaloniki, Greece, August 18–28.

IGME (2015) ZESIS: Base de Datos de Zonas Sismogénicas de la Península Ibérica y territorios de influencia para el cálculo de la peligrosidad sísmica en España. http://info.igme.es/zesis. Accessed October 2020

Jayaram N, Lin T, Baker JW (2011) A computationally efficient ground-motion selection algorithm for matching a target response spectrum mean and variance. Earthq Spectra 27(3):797–815

Jeremias FT, Carvalho A, Coelho AG, Costa AC,(2012) Seismological studies for definition of design earthquake for hydroelectric scheme of Foz Tua site, XIII National Congress of Geotechnical, Lisbon, Portugal, 17–20.

Ji Y, Wu W, Zhao Z (2019) Unloading-induced rock fracture activation and maximum seismic moment. Eng Geol 262:1–13

Jiménez MJ, García-Fernández M (1999) GSHAP Ibero-Maghreb Working Group Seismic hazard assessment in the Ibero-Maghreb region. Annali di Geofisica 42:1057–1065

Joshi V, Chopra S, Kumar S (2020) A local magnitude scale ML for the Saurashtra horst: an active intraplate region, Gujarat, India. J Earth Syst Sci 129:1–9
Kodur VKR, Naser MZ (2013) Importance factor for design of bridges against fire hazard. Eng Struct 54:207–220
Kono Y, Nakamoto K, Hiramatsu Y (2020) Temporal variation in seismic moment release rate of slow slips inferred from deep low-frequency tremors in the Nankai subduction zone, earth. Planets and Space 72:1–9
Kramer SL (1996) Geotechnical earthquake engineering, 1st edn. Prentice-Hall, Upper Saddle River, New Jersey, p 653
Kutanis M, Ulutas H, Isik E (2018) PSHA of Van province for performance assessment using spectrally matched strong motion records. J Earth Syst Sci 127:1–14
Le Goff B, Borges JF, Bezzeghoud M (2014) Intensity-distance attenuation laws for the Portugal mainland using intensity data points. Geophys J Int 199:1278–1285
Lior I, Ziv A (2018) The relation between ground motion, earthquake source parameters, and attenuation: implications for source parameter inversion and ground motion prediction equations. J Geophys Res Solid Earth 123:5886–5901
Luque L, Lario J, Zazo C, Goy JL, Dabrio CJ, Silva PG (2001) Tsunami deposits as paleoseismic indicators example from the Spanish coast. Acta Geologicahispanica 36:197–211
Luzi L, Puglia R, Russo E and ORFEUS WG5 (2016) Engineering Strong Motion (ESM) database, version 1.0. Istituto Nazionale di Geofisica e Vulcanologia, Observatories and Research Facilities for European Seismology. Accessed May 2020. http://esm.mi.ingv.it.
Ma J, Dong L, Zhao G, Li X (2019a) Ground motions induced by mining seismic events with different focal mechanisms. Int J Rock Mech Min Sci 116:99–110
Ma J, Dong L, Zhao G, Li X (2019b) Qualitative method and case study for ground vibration of tunnels induced by fault-slip in underground mine. Rock Mech Rock Eng 52:1887–1901
Matias LM, Cunha T, Annunziato A, Baptista MA, Carrilho F (2013) Tsunamigenic earthquakes in the Gulf of Cadiz: fault model and recurrence. Nat Hazards Earth Syst Sci 13:1–13
McGarr A (1991) On a possible connection between three major earthquakes in California and oil production. Bull Seismol Soc Am 81:948–970
Mert A, Fahjan YM, Hutchings LJ, Pinar A (2016) Physically based probabilistic seismic hazard analysis using broadband ground motion simulation: a case study for the Prince Islands Fault. Marmara Sea, Earth, Planet and Space 68:1–26
Ministerio delle Infrastructure, NTC (Nuove Norme Tecniche per le Construzioni), D.M. 14.09.2005, Ministerio delle Infrastructure, Rome, Italy, 2008.
Mulargia F, Stark PB, Geller RJ (2017) Why is probabilistic seismic hazard analysis (PSHA) still used. Phys Earth Planet Inter 264:63–75
Sistema Nacional de Informação de Recursos Hidricos (SNIRH), database. Accessed May 2020, https://snirh.apambiente.pt/index.php?idMain=4&idItem=2
Pailoplee S, Sugiyama Y, Charusiri P (2009) Deterministic and probabilistic seismic hazard analyses in Thailand and adjacent areas using active fault data. Earth Planets Space 61:1313–1325
Peláez JA, Delgado J, Casado CL (2005) A preliminary probabilistic seismic hazard assessment in terms of Arias intensity in southeastern Spain. Eng Geol 77:139–151
Poljansek K, Marin Ferrer M, De Groeve T, Clark I (2017) Science for disaster risk management, knowing better and losing less, Disaster Risk Management Knowledge Centre (DRMKC). Eur Union Luxemb 2017:554
Portuguese Institute of Sea and Atmosphere (IPMA). Accessed on 17/05/2020. http://www.ipma.pt/pt/geofisica/sismicidade/
Pozos-Estrada A, Liu TJ, Gomez R, Hong HP (2016) Seismic design and importance factor: benefit/cost for overall service time versus per unit service time. Struct Saf 58:40–51
Putti SP, Satyam N (2020) Evaluation of site effects using HVSR microtremor measurements in Vishakhapatnam (India). Earth Syst Environ 4:439–454
Qadri SMT, Malik OA (2021) Establishing site response-based microzonation by applying machine learning techniques on ambient noise data: a casa study from Northern Potwar region Pakistan. Environ Earth Sci 80:1–15
Qadri SMT, Sajjad SH, Sheikh RA, Rehman K, Rafi Z, Nawaz B, Haider W (2015) Ambient noise measurements in Rawalpindi-Islamabad, twin cities of Pakistan: a step towards site response analysis to mitigate impact of natural hazard. Nat Hazard 78:1111–1123
Qadri SM, Nawaz B, Sajjad SH, Sheikh RA (2015b) Ambient noise *H*/*V* spectral ratio in site effects estimation in Fateh jang area, Pakistan. Earthq Sci 28:87–95
Qadri SMT, Islam MA, Shalaby MR, Khattak KR, Sajjad SH (2017) Characterizing site response in the Attock Basin, Pakistan, using microtremor analysis. Abar J Geosci 10:1–11
Ren J, Zhang S (2013) estimation of recurrence interval of large earthquake on the central Longmen Shan fault zone based on seismic moment accumulation/release model. Hindawi Publ Corp 1–8:2013
Ross SM (2008) Probability and statistics for engineers and scientists. Apogeo Editor, Italy, p 614
Sabetta F, Lucantoni A, Bungum H, Bommer JJ (2005) Sensitivity of PSHA results to ground motion prediction relations and logic-tree weights. Soil Dyn Earthq Eng 25:317–329
Scordilis EM (2006) Empirical global relations converting M_s and m_b to moment magnitude. J Seismolog 10:225–236
Seismosignal Software Version 4.0.0 (2010) Seismosoft Ltd, Pavia, Italy
Silacheva NV, Kulbayeva UK, Kravchenko NA (2018) Probabilistic seismic hazard assessment of Kazakhstan and Almaty city in peak ground accelerations. Geodesy and Geodynamics 9:131–141
Sorensen MB, Pulido N, Atakan K (2007) Sensitivity of ground-motion simulations to earthquake source parameters: a case study for Istanbul Turkey. Bull Seimsologicla Soc Am 97:881–900
Sousa ML, Costa AC (2009) Ground motion scenarios consistent with probabilistic seismic hazard disaggregation analysis. Application to Mainland Portugal. Bull Earthquake Eng 7:127–147
Sousa ML, Oliveira CS (1997) Hazard mapping based on macroseismic data considering the influence of geological conditions. Nat Hazards 14:207–225
De Sousa RR, Costa AC, Costa A (2019) Metodologia para a Avaliação da Segurança Sísmica de Edifícios Existentes baseada em Analises de Fiabilidade Estrutural. Technical report 81/2019 – DE/NESDE, LNEC, Portugal, p 148
Soysal BF, Ay BÖ, Arici Y (2017) Evaluation of the ground motion scaling procedures for concrete gravity dams. Procedia Engineering 199:844–849
Stein S, Wysession M (2005) An introduction to seismology, earthquakes, and earth structure. Blackwell Publishing Ltd., p 515
Thiebot E, Gutscher MA (2006) The Gibraltar Arc seismogenic zone (part 1): constraints on a shallow east dipping fault plane source for the 1755 Lisbon earthquake provided by seismic data, gravity and thermal modeling. Tectonophysics 426:135–152
Valentini A, Pace B, Boncio P, Visini F, Pagliaroli A, Pergalani F (2019) Definition of seismic input from fault-based PSHA: remarks after the 2016 central Italy earthquake sequence. Tectonics 38:595–620

Vrettos C (2013) Dynamic response of soil deposits to vertical SH waves for different rigidity depth-gradients. Soil Dyn Earthq Eng 47:41–50

Wennerberg L (1990) Stochastic summation of empirical Green's functions. Bull Seismol Soc Am 80:1418–1432

Woessner J et al (2015) The 2013 European seismic hazard model: key components and results. Bull Earthquake Eng 13:3553–3596

Wolfram Mathematica 12, Software, Version 12.0, Wolfram Research, Inc., 2019.

Wu YM, Chen SK, Huang TC, Huang HH, Chao WA, Koulakov I (2018) Relationship between earthquake *b*-values and crustal stresses in a young orogenic belt. Geophys Res Lett 45:1–6

Yan F, Xu K, Yao X, Li Y (2016) Fuzzy Bayesian network-bow-tie analysis of gas leakage during biomass gasification. PLoS ONE 11:1–21

Zacchei E, Molina JL (2020) Reviewing arch-dams' building risk reduction through a sustainability-safety management approach. Sustainability 12:1–24

Zacchei E, Molina JL (2021) Introducing importance factors (IFs) to estimate a dam's risk of collapse produced by seismic processes. Int J Disaster Risk Reduction 60:1–13

Zacchei E, Molina JL, Brasil R (2017) Seismic hazard assessment of arch dams via dynamic modelling: an application to the Rules Dam in Granada SE Spain. Int J Civil Eng 1–10:2017

Zacchei E, Molina JL (2020) Artificial accelerograms to estimate damage of dams by using failure criteria. Scientia Iranica 27:2740–2751. https://doi.org/10.24200/sci.2018.50699.1824

Zhan Z (2017) Gutenberg-Richter law for deep earthquakes revisited: a dual-mechanism hypothesis. Earth Plan Scie Lett 461:1–7. https://doi.org/10.1016/j.epsl.2016.12.030